Article:

Hasanali, M., Mojtabaei, S.M. orcid.org/0000-0002-4876-4857, Clifton, G.C. et al. (3 more authors) (2022) Capacity and design of cold-formed steel warping-restrained beam-column elements. Journal of Constructional Steel Research, 190. 107139. ISSN 0143-974X

https://doi.org/10.1016/j.jcsr.2022.107139

Capacity and design of cold-formed steel warping-restrained beam-column elements

Maryam Hasanali[a*], Seyed Mohammad Mojtabaei[b], G.Charles Clifton [a], Iman Hajirasouliha[b], Shahabeddin Torabian[c], James B.P. Lim[a]

[a] Department of Civil and Environmental Engineering, The University of Auckland, New Zealand

[b] Department of Civil and Structural Engineering, The University of Sheffield, Sheffield, UK

[c] Department of Civil Engineering, Johns Hopkins University, Baltimore, MD, USA

[*] Corresponding author: mhas455@aucklanduni.ac.nz

Abstract

In current design standards, cold-formed steel (CFS) beam-column elements are generally designed by considering fully warping free behaviour in their supports, which means the benefit of warping-restrained boundary conditions is neglected. In addition, while a non-linear relationship governs the interaction of axial compression and bending, simplified linear expressions are prescribed in design standards, which may lead to unreliable designs. This paper aims to investigate the efficiency of the well-known Direct Strength Method (DSM) as well as the methods proposed by previous researchers for CFS warping-restrained beam-column members. The results of experimentally validated warping-restraint Finite Element (FE) models, considering material nonlinearity and geometric imperfections, are used as a benchmark. A total of 270 CFS elements with various lengths, thicknesses and cross-sectional dimensions are considered under ten different load eccentricity levels. The results are then employed to investigate the effects of warping-restrained boundary conditions as well as code recommended interaction curves on the efficiency of the existing methods to estimate the strength of CFS beam-columns with warping restraint. The results indicate that the estimated capacity of CFS beam-columns is significantly affected (up to 55%) by the warping restraint effects and the errors associated with using the simple linear interaction curve, depending on the element length and thickness. While the influence of warping restraint is generally less than 6%, it is demonstrated that, on average, all existing design methods underestimate the capacity of CFS beam-columns by at least 20%, which highlights the need to develop more accurate design methods for practical design purposes.

Keywords: Cold-formed steel, Beam-columns, Warping-restrained boundary conditions, Direct Strength Method (DSM), Finite element (FE) model

1 Introduction

Cold-formed steel (CFS) members have been traditionally employed as secondary elements, such as roof purlins, wall girts and cladding or as wall studs in non-structural internal walls in multi-storey buildings. However, CFS members are increasingly being used in the structural systems of low to mid-rise buildings, including shear-wall panels and moment-resisting portal frames [1, 2] due to their structural and environmental advantages, such as their high strength-to-weight ratio, flexibility in cross-sectional shapes, ease of assembly, transportation and recyclability [3].

In most structural system applications, CFS structural members are subjected to combined axial compression and bending (see Fig. 1(a)) both in moment resisting frames [4, 5] and stud wall systems [6, 7]. CFS compression members are also highly susceptible to eccentric loads due to their thin-walled open cross-sections, an example as shown in Fig. 1(b). This can generate combined axial compression and bending moments and consequently alter the behaviour and failure mechanism of CFS members [8-10].

The behaviour of CFS beam-column members under various load combinations has been experimentally and numerically investigated in the literature. Torabian et al. [9, 10] conducted

55 experimental tests on warping restrained lipped channel-sections and 43 tests on Z-sections under axial compression and bi-axial moments; using the results of these tests the reliability of the American Iron and Steel Institute (AISI S100 (2012)) [11] was assessed. They showed that the use of linear interaction expressions for the beam-columns is excessively conservative. In another study, Cheng et al. [12] analytically investigated lateral-torsional buckling of CFS lipped channel sections subjected to combined axial compression and bending about their major and minor axes. It was demonstrated that the bending moment decreases the critical compression load for a section subject to combined compression and the major-axis bending, while the effect of minor-axis bending moment on the critical compression load depends on the direction of applied bending. The critical value of the compression load will be reduced when the direction of minor axis bending moment puts the lips into compression, whereas the direction of bending moment creating the compression in the web has almost no effect on the critical value of the compression load, unless the magnitude of the applied moment is very close to the design member moment capacity. A comprehensive experimental program was conducted by Ma et al. [13] on 51 high-strength CFS beam-column elements with square and rectangular hollow sections and the results were used to compare the accuracy of the predictions obtained from American [14], European [15], and Australian design provisions [16]. More recently, Li and Young [17] experimentally investigated the behaviour of 33 CFS built-up open section beam-columns under different eccentric loads. They reported that the AISI S100 (2016) [21], AS/NZS 4600 (2018) [22], EN 1993-1-1 (2005) [15] and ANSI/AISC 360 (2010) [14] generally underestimate the strengths of the CFS built-up beam-column members. With regards to the optimisation of CFS beam-column elements, a number of research studies were also devoted to identify optimum cross-sectional shapes and dimensions of single and built-up beam-columns to maximise their load-bearing capacity under various load combinations [18-20].

The majority of these experimental studies focused on CFS beam-column members with restrained warping at their supports, which is consistent with the way these elements are generally used in the construction practice (e.g., studs in shear wall panels). However, the AISI S100 (2016) [21] and AS/NZS 4600 (2018) [22] only prescribe simple linear interaction equations for beam-column elements. To address this issue, Moen [23] and Rajkannu and Jayachandran [24] proposed different methods to take into account the effects of warping restraint in CFS compressive members. However, these methods were developed based on limited number of cases; and therefore, there is a need to assess their efficiency for a wider range of elements and load conditions.

This paper aims to provide a better understanding about the effects of warping-restrained boundary conditions on the behaviour and failure mechanism of CFS beam-column elements and evaluate the reliability of the Direct Strength Method (DSM) as specified in AISI S100 (2016) [21] and AS/NZS 4600 (2018) [22] as well as design proposals found in the literature. To this end, detailed nonlinear Finite Element (FE) models of CFS beam-column members under different load combinations are developed by taking into account material nonlinearity and geometric imperfections and validated based on the results of existing experimental tests. The validated models are then used for the parametric studies on the key design parameters of beam-column members, including length (i.e., 0.5, 1.5, 3 m), thickness (i.e., 1, 2, 4 mm) and cross-sectional dimensions subjected to ten different load eccentricities (in total 270 specimens). The results are then employed to investigate the effects of warping-restrained boundary conditions on the strength of CFS beam-columns and subsequently assess the interactions curves and accuracy of the existing methods for estimation of their capacity.

2 Current design methods for CFS members

The two main methodologies which are generally available in the current design guidelines for CFS members are the Effective Width Method (EWM) (AISI 1996) [25] and the Direct Strength Method (DSM) (AISI 2004) [26]. While the DSM is mainly adopted in AISI S100 (2016) [21] and AS/NZS 4600 (2018) [22], the EWM is prescribed in the majority of CFS design standards including EN 1993-1-3 (2006) [27], AISI S100 (2016) [21] and AS/NZS 4600 (2018) [22]. The EWM uses reduced cross-section properties along with the yield stress; however, the DSM employs the gross cross-section properties in conjunction with a direct reduced strength based on the stability of the gross cross-section [28]. The comparison between the strength predictions of EWM and DSM against the experimental results of lipped channel columns revealed that the test-to-predicted ratio can vary from 0.6 to 1.3 [28, 29]. In a recent study, a framework was developed to predict the axial capacity of CFS channel sections using Deep Belief Network (DBN) [30]. Comparison of the results with the EWM and DSM estimations confirmed that these methods are generally conservative by around 15%.

2.1 DSM

The Direct Strength Method was first presented by Schafer and Peköz [29] as an alternative to the traditional effective width method to predict the load-carrying capacities of CFS members. In this method, the capacity of a CFS member is determined by utilizing the yield strength of the member and the elastic stability of the cross-section (i.e., local, distortional, and global buckling) using empirical relationships. To predict elastic critical buckling strength, finite strip analysis is performed by using CUFSM [32] or Thin-Wall [33] software. In this section, the prediction of buckling resistance for different warping-free CFS structural elements (i.e., column, beam and beam-column) are briefly described.

2.1.1 Buckling resistance of column elements

According to AISI S100 (2016) [21], axial compressive resistance for global buckling is expressed in terms of compressive yield load, $P_y = A_g f_y$, and slenderness ratio $\lambda_c = \sqrt{P_y/P_{cre}}$ (where A_g is the gross cross-sectional properties, f_y is the yield stress, and P_{cre} denotes the elastic global buckling strength):

$$\begin{cases} P_{ne} = \left(0.658^{\lambda_c^2}\right)P_y & for\ \lambda_c \leq 1.5 \\ P_{ne} = \left(\frac{0.877}{\lambda_c^2}\right)P_y & for\ \lambda_c > 1.5 \end{cases} \tag{1}$$

where P_{ne} is the nominal member compression capacity for flexural, torsional, and flexural-torsional buckling.

AISI S100 (2016) [21] takes into account the local-global interaction mode through the local-global slenderness ratio $\lambda_l = \sqrt{P_{ne}/P_{crl}}$, and therefore, the nominal axial resistance for local buckling is defined by [21]:

$$\begin{cases} P_{nl} = P_{ne} & for\ \lambda_l \leq 0.776 \\ P_{nl} = [1 - 0.15\left(\frac{P_{crl}}{P_{ne}}\right)^{0.4}]\left(\frac{P_{crl}}{P_{ne}}\right)^{0.4} P_{ne} & for\ \lambda_l > 0.776 \end{cases} \tag{2}$$

The nominal axial resistance for distortional buckling is expressed in terms of distortional buckling slenderness ratio $\lambda_d = \sqrt{P_y/P_{crd}}$:

$$\begin{cases} P_{nd} = P_y & for\ \lambda_d \leq 0.561 \\ P_{nd} = [1 - 0.25\left(\frac{P_{crd}}{P_y}\right)^{0.6}]\left(\frac{P_{crd}}{P_y}\right)^{0.6} P_y & for\ \lambda_d > 0.561 \end{cases} \tag{3}$$

The nominal axial resistance of the compression member (P_n) is then predicted by using the minimum value of the resistances determined in Eqs. (1) to (3).

2.1.2 Buckling resistance of beam elements

Based on AISI S100 (2016) [21] regulations, the nominal flexural resistance is determined through the flexural yield moment $M_y = W_y f_y$ and the elastic critical lateral-torsional moment M_{cre} (where W_y is the elastic section modulus, termed Z_y in AS/NZS 4600 [22]):

$$\begin{cases} M_{ne} = M_{cre} & for\ M_{cre} < 0.56M_y \\ M_{ne} = \dfrac{10}{9} M_y \left(1 - \dfrac{10M_y}{36M_{cre}}\right) & for\ 2.78M_y \geq M_{cre} \geq 0.56M_y \\ M_{ne} = M_y & for\ M_{cre} > 2.78M_y \end{cases} \tag{4}$$

The nominal flexural resistance for local buckling considering local-global interaction is also expressed as a function of the local-global slenderness ratio $\lambda_l = \sqrt{M_{ne}/M_{crl}}$:

$$\begin{cases} M_{nl} = M_{ne} & for\ \lambda_l \leq 0.776 \\ M_{nl} = [1 - 0.15\left(\dfrac{M_{crl}}{M_{ne}}\right)^{0.4}]\left(\dfrac{M_{crl}}{M_{ne}}\right)^{0.4} M_{ne} & for\ \lambda_l > 0.776 \end{cases} \tag{5}$$

The nominal flexural resistance for distortional buckling is determined using distortional buckling slenderness ratio $\lambda_d = \sqrt{M_y/M_{crd}}$:

$$\begin{cases} M_{nd} = M_y & for\ \lambda_d \leq 0.673 \\ M_{nd} = [1 - 0.22\left(\dfrac{M_{crd}}{M_y}\right)^{0.5}]\left(\dfrac{M_{crd}}{M_y}\right)^{0.5} M_y & for\ \lambda_d > 0.673 \end{cases} \tag{6}$$

The nominal flexural resistance of the CFS member (M_n) is then obtained from the minimum value of the resistances determined in Eqs. (4) to (6).

2.1.3 Buckling resistance of beam-column elements

AISI S100 (2016) [21] recommends two linear interaction equations for the warping-free CFS members under combined axial compression and bending moments:

$$\frac{P}{P_n} + \frac{M_x}{M_{nx}} + \frac{M_y}{M_{ny}} \leq 1.0 \quad (7)$$

In the above equation P, M_x and M_y are defined as the applied axial compression load and bending moments about the x and y-axes, respectively. P_n is denoted as available axial compressive capacity, while M_{nx} and M_{ny} are available flexural strength about the x and y-axes, respectively.

2.2 DSM with warping-restrained elastic Buckling resistances

To take into account the effects of warping restrained boundary conditions, the elastic critical buckling loads and bending moments of the DSM equations can be replaced with those obtained for warping restrained boundary conditions [19]. Based on this method, the warping restrained CFS element can be modelled in Finite Element (FE) software (e.g., ABAQUS [34]) under pure axial load and pure bending moments in major and minor axes. The eigenvalues obtained from the FE analyses are then employed to predict the capacities through the DSM equations.

2.3 Proposed design method by Moen

Moen [23] investigated the effects of warping deformation on the column cross-sections through experimental and analytical studies and reported that the warping-fixed boundary conditions can lead to shortening the distortional buckling half-wavelength. This results in an amplification of the elastic critical distortional buckling load (P_{crd}) of the column members. It was also demonstrated that the magnitude of the boost in P_{crd} decreases by increasing the column length, since the wavelength shortening required to accommodate distortional buckling in the column can be distributed over multiple half-waves in which the flange can rotate in plan going from one half wavelength into the adjacent half wavelength.

Based on the results of their study, Moen [23] updated DSM equations for warping restrained CFS columns by proposing a boosting factor that enhances the elastic critical distortional buckling load (P_{crd}), while the critical elastic local buckling load (P_{crl}) remains unchanged. The boosting factor, which is applied on the distortional critical buckling load (P_{crd}), is given by Eq. (8), where L_{crd} is the distortional half-wavelength and L is unbraced length of the member.

$$D_{boost} = 1 + \frac{1}{2}\left(\frac{L_{crd}}{L}\right)^2 \tag{8}$$

2.4 Proposed design method by Rajkannu & Jayachandran

In a more recent study, Rajkannu and Jayachandran [24] studied the effects of warping on the flexural-torsional buckling behaviour of the CFS lipped-channel sections under pure axial compression experimentally and numerically. It was concluded that the compressive strength and failure modes may significantly change by restraining warping, and consequently, the current DSM predictions for flexural-torsional buckling strength can be very conservative. In this study, warping restraint factors w_i and w_e for inelastic and elastic region, respectively, were proposed as given in Eq. (9) to modify the strength predicted by DSM for global buckling of the axial compressive element (P_{ne}).

$$P_{ne} = \begin{cases} (w_i \times 0.658^{\lambda_c^2})P_y & for\ \lambda_c \le 1.5 \\ \left(\dfrac{w_e \times 0.877}{\lambda_c^2}\right)P_y & for\ \lambda_c > 1.5 \end{cases} \tag{9}$$

In the above equation, w_i = w_e= 1 for the members failing in flexure buckling, and w_i =1.27, w_e= 1.9 for the members failing in flexural-torsional buckling.

To predict the dominant buckling mode, a threshold was proposed using the ratio x_o/b, where x_o is the distance between the centroid and shear centre of the cross-section and b is the cross-sectional flange width. If $x_o/b > 0.75 + 0.7(d/b)$, the member fails in flexural-torsional buckling (d is the dimension of cross-sectional lips), while the member fails in flexural buckling if $x_o/b < 0.75 + 0.7(d/b)$. It was demonstrated that the strength of members failing in flexural buckling is independent of the warping restraint conditions. It should be mentioned that this method failed to consider the effects of the warping-fixed boundary condition on the capacity of the members studied herein as none of the failure modes of these cross-sections was flexural-torsional buckling in compression loading conditions.

2.5 Proposed design method by Torabian and Schafer

While the design of CFS beam-column members is on the basis of a linear interaction of axial compression and bending moments, Torabian & Schafer [8] and Torabian et al. [9] extended the DSM in order to take into account the actual stresses generated by combined actions. In fact, the actual stress distributions resulted from both compression and bending are used in a buckling analysis to determine the critical buckling parameters [8]. In this method, the applied axial compression and bending moments are first normalised to the cross-sectional yield strength (M_{1y}, M_{2y}, P_y), and then the normalized points are shifted from x, y and z coordinates to an azimuth angle (θ_{MM}), an elevation angle ($\emptyset_{PM}$) and a radial length (β), respectively:

$$\theta_{MM} = \tan^{-1}({}^{y}/_{x}), \emptyset_{PM} = \cos^{-1}({}^{z}/_{\beta}), \beta = \sqrt{x^2 + y^2 + z^2} \tag{10}$$

For any required action ($P_r - M_{1r} - M_{2r}$), the following parameters are defined:

$$x_r = \frac{M_{1r}}{M_{1y}}, y_r = \frac{M_{2r}}{M_{2y}}, z_r = \frac{P_r}{P_y} \tag{11}$$

$$\theta_{MM} = \tan^{-1}(y_r/x_r), \emptyset_{PM} = \cos^{-1}(z_r/\beta_r), \beta_r = \sqrt{x_r^2 + y_r^2 + z_r^2} \tag{12}$$

Therefore, the state of the stress on the cross-section can be determined as follows:

$$\sigma_r = \frac{P_r}{A} + \frac{M_{1r} y_{c2}}{I_1} + \frac{M_{2r} y_{c1}}{I_2} \tag{13}$$

where σ_r is the required axial stress under combined required actions (P_r , M_{1r} and M_{2r}), y_{c1} and y_{c2} are the distance to the centroidal principal axes 1 and 2, respectively, and A, I_1, and I_2 are the cross-sectional area, and the moment of inertia about axes 1 and 2, respectively.

By obtaining the maximum required axial stress σ_{r-max} from Eq. (13), the yielding actions $(\beta_y, \theta_{MM}, \emptyset_{PM})$ can be determined as follows:

$$|\sigma_r(y_{c1}, y_{c2})|_{max} \times \alpha_y = F_y \tag{14}$$

$$\alpha_y = \frac{F_y}{\sigma_{r-max}} \tag{15}$$

$$\beta_y = \alpha_y \beta_r \tag{16}$$

where F_y is the yield stress, β_y represent the first yield of the members. Cross-section stability analysis performed on σ_r provides elastic buckling load factors for local (α_{crL}), distortional (α_{crD}) and global (α_{crG}) buckling. Using the elastic buckling load factor, elastic buckling strength under the combined actions $(\beta_r, \theta_{MM}, \emptyset_{PM})$ are as follows:

$$\beta_{crL} = \alpha_{crL} \beta_r \tag{17}$$

$$\beta_{crD} = \alpha_{crD} \beta_r \tag{18}$$

$$\beta_{crG} = \alpha_{crG} \beta_r \tag{19}$$

where β_{crG} , β_{crD} and β_{crL} show the elastic buckling values for global, distortional and local elastic buckling, respectively. Nominal strength (β_n) is, therefore, the minimum of the member strength in local, distortional and global buckling.

3 Description of Finite Element (FE) models

FE analysis has been frequently proved to be an efficient tool in predicting the behaviour and strength of CFS elements and structural components [35-37]. In this study, detailed nonlinear FE models of CFS elements under various loading conditions have been developed using ABAQUS software [34] by considering the material nonlinearity and geometric imperfections. The models have then been validated based on the results of two experimental programs: (i) CFS elements under pure axial compression (i.e. columns) tested by Ye et al. [38] at the University of Sheffield and (ii) CFS elements under combined axial compression and bending moments (i.e., beam-columns) conducted by Torabian et al. [39] at Johns Hopkins University. It should be mentioned that while Torabian et al. [39] also conducted pure axial compression tests, they did not obtain good agreements between the results of their experiments and the corresponding FE models, due to some uncertainties such as the existence of the global twist imperfection. Therefore, it was decided to use two different experimental tests to validate the FE models adopted in this study.

3.1 Specimens, boundary conditions and loading

Ye et al. [38] tested pined-ended warping-restrained CFS columns with different lengths and cross-sectional dimensions under concentric axial compressive loads. To simulate the adopted test setup, a 38 mm thick solid plate with an arc-shaped groove and a cylinder roller with a radius of 12 mm embedded inside the groove were modelled at both ends of the specimens as the hinge assemblies, as shown in Fig. 2. The contacts were defined between: (i) the column specimen and the endplate and (ii) the roller and end plate (see Fig. 2). A node-to-surface contact pair was used to define the interaction between the column specimen and the endplate, where combined "hard" and "rough" contact behaviour were assigned in normal and tangential directions to avoid any penetration and tangential slip between the surfaces, respectively [34]. A surface-to-surface contact property was also used to define the interaction of the endplate and roller. While "hard" contact was defined in the normal direction, the contact in the tangential direction was set to "penalty" to take into account the effects of friction between the roller and endplate. Based on the sensitivity analyses conducted in [31], the most appropriate friction factor to achieve convergence was obtained to be equal to 0.2. The sensitivity analysis demonstrated that the predicted compressive capacity decreases with the reduction of friction factor, whereas no significant drop of the peak load was observed using friction factors smaller than 0.2. Moreover, a friction factor of 0.2 provided an excellent agreement between the experimental and numerical results. At each end of the member, the nodes of the top surface of the roller which is in contact with the groove were coupled to the reference point with fixed boundary conditions.

Torabian et al. [39] tested a set of CFS beam-column members under eccentric axial compressive loads in order to generate combined actions (i.e., compression and bending moments) on the elements. One reference point was placed at each end of the member and the coordinate of the reference point was varied as different eccentricities applied to the specimen. A rigid link with a length of 152.4 mm was created between the reference point and the specimen end to simulate the depth of the clevis used in the test set-up. All degrees of freedom of each end cross-section were then coupled to its corresponding reference point pined about the minor and major axis, as shown in Fig. 3.

3.2 Element type and material properties

A nine-node shell element with reduced integration, $S9R5$, selected from the ABAQUS element library [34] was assigned to both column and beam-column members. Each node of this element type has three translational degrees of freedom and two in-surface rotational degrees of freedom. Based on the investigations conducted by Schafer et al. [41], this element type can provide accurate predictions for thin-walled structures. An 8-node linear brick element with reduced integration ($C3D8R$) and hourglass control was also used for the modelling of the endplates and rollers. Following a comprehensive mesh sensitivity analysis, the element sizes of 10×10 mm^2 were found to be suitable for the flat regions of the CFS columns under pure compression and beam-column elements subjected to combined compression and bending moments, while four elements were used in the radial direction of the corners. To show the results of mesh sensitivity analysis, the load-displacement responses of one of the CFS members (i.e., B1500-c cross-section adapted from Ye et al. [38]) with various mesh sizes are demonstrated in Fig. 4.

In general, the ultimate capacity and post-buckling behaviour of CFS elements can be significantly affected by the inelastic properties of CFS material [40]. In this study, the behaviour of CFS elements was simulated by using a bi-linear stress-strain model. To model the CFS column elements, the elastic Young's modulus of E =196 GPa and the yield stress of F_y = 440 MPa were used based on the results of coupon tests [38]. Similarly, the measured elastic Young's modulus of E =203.4 GPa and the yield stress of F_y = 365 MPa were also used for beam-column members [39]. The Poisson ratio was taken equal to 0.3 for both column and beam-column members. It should be noted that the obtained engineering stress-strain curves were converted to true stress and true strain data using the following equation:

$$\begin{cases} \varepsilon_{true} = \ln(1 + \varepsilon_e) \\ \sigma_{true} = \sigma_e(1 + \varepsilon_e) \end{cases} \quad (20)$$

where σ_e and ε_e are the measured engineering stress and strain data based on the original cross-sectional area of the coupons. Fig. 5 compares the engineering and the true stress-strain curves of the tested column and beam-column elements.

With respect to the roll-forming/cold-work effect, generally cold-formed structural sections are manufactured by rolling process, causing residual stress and increasing the material yield stress in the corner zones. It has previously been demonstrated that the effects of membrane residual stresses can safely be neglected in open sections [40, 41] while the (longitudinal) bending residual stresses are implicitly accounted for in the coupon test results, provided that the coupons are cut from the fabricated cross-section rather than from the virgin plate. Indeed, cutting a coupon releases the bending residual stresses, causing the coupon to curl [41]. However, these stresses are re-introduced when the coupon is straightened under tensile loading in the initial stages of the coupon test.

3.3 Geometric imperfections

It has been previously shown that the initial geometric imperfections can have considerable effects on the strength and post-buckling behaviour of CFS elements [42, 43]. The general shape of imperfections can be generally determined according to the dominant buckling mode shape (i.e., local, distortional, and global) obtained from elastic buckling analysis [29]. In this study, the Finite Strip Method was first performed through CUFSM software [32] to predict the dominant buckling mode shape and its corresponding half-wavelength for each element. Following the above procedure, a program was developed in Matlab [44] for the inclusion of imperfections and generating of nodal coordinates in ABAQUS [34]. The magnitude of the cross-sectional deformed shape was then scaled to certain values depending on the thickness of the elements. Based on the work conducted by Schafer and Peköz [40] for cross-sections with a thickness (t) smaller than 3 mm, the amplitudes of imperfections for local and distortional buckling were taken as $0.34t$ and $0.94t$, respectively, corresponding to a Cumulative Distribution Function (CDF) value of 50%. For specimens with a thickness (t) larger than 3 mm, the imperfection magnitude was determined using the following equation proposed by Walker [45]:

$$\omega_d = 0.3t\sqrt{\frac{\sigma_{0.2\%}}{\sigma_{cr}}} = 0.3t\lambda_s \qquad (21)$$

where $\sigma_{0.2\%}$ and σ_{cr} are 0.2% proof stress of the material and elastic critical local/distortional buckling stress of the cross-section; respectively, and λ_s is the cross-sectional slenderness, given by:

$$\lambda_s = \sqrt{f_y/\sigma_{cr}} \quad (22)$$

The amplitude of geometric imperfection for global buckling, which is in the shape of a half-sine wave, was taken as $L_e/\ 1500$, as reported in previous studies [31, 46] (where L_e is the length of the member). While local and/or distortional buckling modes were identified to be dominant for the short elements [31], a combination of three buckling modes (i.e. local, distortional and global) was introduced for the medium and long length members [39].

3.4 Validation of the FE models

To predict the capacity of the CFS elements, nonlinear inelastic post-buckling analysis was performed by using the standard RIKS arc-length method in ABAQUS [34]. Table. 1 lists the strength of the CFS column members under pure axial compression obtained from FE models (P_{FE}) and the tests (P_{Test}) [38] for three various lengths (1000, 1500 and 2000 mm) and four different cross-sectional dimensions (A, B, C and D), as shown in Fig. 6(a). Similarly, Table. 2 compares the strength obtained from FE and the tests for CFS beam-column members with three various element lengths (305, 610 and 1219 mm) subjected to compressive loads with nine different eccentricity values on the minor (y) and major axes (x). The beam-column members were consequently subjected to the combined actions of (i) compression and minor axis bending moment, (ii) compression and major axis bending moment and (iii) compression and biaxial bending moments. The cross-sectional dimensions of these beam-column specimens are shown in Fig. 6(b). It should be noted that all demonstrated dimensions are reported out-to-out dimensions.

In general, good agreements were achieved between the strength and failure mechanism of the FE models and the corresponding experimental tests. The results demonstrated that the developed FE models could accurately predict the strength of the column and beam-column elements with maximum estimation errors of 8% and 4% with the standard deviations of 0.05 and 0.02, respectively. For instance, Figs. 7 and 8 demonstrate that the failure modes predicted by the developed FE models compare very well with those observed during the experimental tests on A1000-a (column element) under axial load and S600-1219-15 (beam-column element) under combined compression and bi-axial bending moments. These two elements failed in local buckling first, followed by the interaction of local and overall flexural buckling about the minor axis. In addition, Fig. 9 compares the axial force-displacement relationship for A1000-a and S600-610-8 specimens obtained from the reference experimental tests and the predicted results from the numerical study. It is demonstrated that the proposed FE models were able to capture the peak load, initial stiffness and post-buckling behaviour of both column and beam-column specimens.

4 Parametric study

The experimentally validated FE models described in the previous section have then been used to conduct a comprehensive parametric study. The purpose of the parametric study is to investigate the effects of warping-restrained boundary conditions on the maximum capacity of CFS structural elements (i.e., columns and beam-columns) and assess the efficiency of the code proposed compression force-bending moment interaction equation as well as the limitations of the current design methods.

In total, 270 CFS elements subjected to 10 different load combinations were selected by considering various key design parameters, including three sets of cross-sectional dimensions ($C1$, $C2$ and $C3$), thicknesses (1 mm, 2 mm and 4 mm) and lengths (500 mm (short), 1500 mm (medium) and 3000 mm (long)), as shown in Table. 3. The same modelling techniques described in Section 3 were adopted for the parametric study. For a fair comparison, similar material properties were considered for CFS column and beam-column elements (E =207 GPa, F_y = 350 MPa, F_u = 600 MPa and Poisson ratio =0.3). Fig. 5(c) demonstrates the bi-linear stress-strain curve used in FE models. The selection of loading conditions was on the basis that the effects of all possible combinations of axial compression force and bending moments can be investigated, including pure compression, combined compression and major axis bending, combined compression and minor axis bending and combined compression and bi-axial bending. This was provided using different values of eccentricities as listed in Table. 4. The failure modes of the selected cross-sections under pure actions are listed in Table. 5, which can be either local, distortional, local-global and yielding. As specified in Eq. 4, the yielding failure in the members subjected to pure bending can be achieved when the calculated elastic critical lateral-torsional moment (M_{cre}) is greater than 2.78 times yield moment (M_y). It should be noted that the dominant failure mode of CFS beam-column members was assumed to be the same as the elements under pure compression, where the dominant mode was determined using the lowest values of the buckling loads obtained from DSM equations (see Section 2). This assumption is generally valid for beam-column elements where the axial behaviour is dominant (which is the case for the specimens considered in this study).

5 Results and discussions

Tables. A1 to A3 in the Appendix A present the strength results of the beam-column members with three different cross-sections ($C1$, $C2$ and $C3$) obtained from the detailed FE models (P_{DFE}) and the four different design methods specified in Section 2, including DSM (P_{DSM}), DSM with warping-restrained elastic buckling resistance ($P_{DSM,W}$), Moen ($P_{Distortional,W}$) [23] and Torabian et al. ($P_{Interaction}$) [39]. These tables also list the values of imposed eccentricities in y (e_y) and x (e_x) directions that generate bending moments about major and minor axes, respectively, ratios of strength predictions obtained from each design method to the detailed FE models, and the calculated statistical indicators.

5.1 Efficiency of the existing design methods

Fig. 10 is used to assess the efficiency of the existing design methods, where average estimation errors in the estimated capacity using the existing design methods in comparison with the detailed FE models are presented under various loading conditions (pure compression, combined compression and minor axis bending with the web in tension or compression, combined compression and major axis bending and combined compression and bi-axial bending). Overall, using existing design methods for the strength calculations of the short CFS member (i.e., 500 mm) results in less accurate predictions compared to medium (i.e., 1500 mm) and long members (i.e., 3000 mm) under combined actions. On the other hand, it is shown that the average ratio of the strength predictions obtained from different design methods and the detailed FE models for the CFS elements under pure compression is 0.87, 0.84 and 0.69 for short, medium, and long length members, respectively. The results also indicate that the DSM led to the most conservative predictions, especially for short members, underestimating the capacity results up to 55% compared to the detailed FE results. This can be attributed to (i) the absence of the warping restrained boundary condition effects, (ii) the DSM equations for the calculations of buckling loads, and (iii) the AISI S100 (2016) [21] linear interaction equation. Based on the results, it can be concluded that the highest estimation error in DSM predictions was observed when the CFS beam-columns were under combined compression and bi-axial bending moments (average estimation errors of 40%, 27% and 19% for short, medium, and long length members, respectively).

With respect to the DSM with warping-restrained elastic buckling resistance ($P_{DSM,W}$), it can be clearly seen that this method provided a better prediction than the DSM in all the three selected lengths (by up to 7.3%), arising to the existence of the warping restrained effect in this method as shown in Fig. 10. However, the maximum difference between the predictions of this method and the detailed FE results was still 51% (see Table. A1), which can be attributed to the estimation errors sourcing from the DSM equations and the AISI S100 (2016) [21] interaction equation as discussed before. This highlights the need for further investigations in this area.

The method proposed by Moen [23], in which the effects of the end boundary conditions are taken into account for the specimens failing in distortional buckling mode, could provide more accurate strength predictions compared to the DSM by up to 16%. It should be noted that in this study only five cross-sections of the short members were prone to the distortional buckling mode ($C1$ with 1-, 2- and 4-mm thickness, and $C2$ and $C3$ with 4 mm thickness), as shown in Table. 5. Therefore, the efficiency of Moen's method can be solely seen in Fig. 10(a) for the short members (i.e., 500 mm), and the results of the DSM and this method are identical for the medium and long length members (see Fig. 10(b) and (c)). Furthermore, the efficiency of the method proposed by Moen [23] was especially evident in the members with a thickness of 4 mm. In general, the average ratio of strength values obtained from Moen method ($P_{Distortional,W}$) and detailed FE results (P_{DFE}) is 0.71. This average ratio reaches 0.69 when the DSM procedures are used, which indicates the Moen's method provides slightly more accurate capacity predictions. The results also demonstrated that the best agreement between the results of this method and the detailed FE predictions was obtained when members were subjected to the pure compression load. This can be justified considering that this method was originally developed for members under pure compression load.

It can be seen that compared to the other design methods, the Torabian et al. method [39] is capable of predicting strength values with a higher level of efficiency in most cases. This is especially evident for the medium length elements, where the load-carrying capacities predicted by this design method are in a reasonable agreement with the detailed FE results with an average underestimated result of 11% (see Fig. 10(b)). In contrast, the most significant estimation error was found in CFS elements with 500 mm length with an average of 25% (see Fig. 10(a)). Fig. 10 also indicates that Torabian et al. method [39] led to better strength predictions when the CFS members are subjected to the combined axial compression and minor axis bending and combined axial compression and bi-axial bending. It should be noted that this method noticeably overestimated the capacities of some of the CFS members, especially those with longer (i.e., 3000 mm) and thicker (i.e., 4 mm) elements (see Tables. A2 and A3).

5.2 Effects of warping-restrained boundary conditions

In order to assess the effects of warping restrained boundary conditions on the capacities of the CFS members, the results of the DSM ignoring the warping-fixed effect and the DSM with warping-restrained elastic buckling resistance are compared in this section. The results demonstrate that restraining warping of CFS elements improved the capacities of the members in all cases (on average by 6%, 2.5% and 1.2% for short, medium and long members), as shown in Fig. 11. It can be noted that while the warping-restrained boundary conditions were more effective for the short CFS elements (see Fig. 11(a)), increasing the element length considerably reduced the effects of warping (see Fig. 11(b) and (c)). This is attributed to the shortening of the buckling half-wavelength caused by the warping-restrained condition, which means the wavelength shortening can be distributed over multiple half-waves as the length of the cross-section increases [23].

In general, it can be concluded that the effects of the warping-restrained on the capacity of CFS elements under combined actions were not significant (less than 7.3%). This indicates that the estimation errors associated with the DSM can be referred to the inefficiency of the AISI S100 (2016) interaction equation [21]. On the other hand, when the CFS elements were under pure axial compression, in the absence of the interaction equation, DSM still predicted the strength with a noticeable estimation error (see Fig. 11). This highlights again the estimation error caused by the DSM equations for the cross-sectional buckling capacities. In particular, the most significant estimation error of DMS was observed for the long length members (i.e., 3000 mm) under pure axial compression (31% on average), in which unlike medium and short length members, local-global buckling was determined as the dominant buckling mode (see Table. 5). This is consistent with the results previously reported by Ye et al. [38] that the DSM takes into account the effects of the local-global buckling mode with a noticeable difference.

5.3 Efficiency of the interaction equation

This section investigates the efficiency of the interaction equation proposed by the AISI S100 (2016) [21] for the members under the combined actions of axial compression load and bending moments. To assess the efficiency of the interaction equation, the effects of the warping-restrained boundary conditions and the inaccuracy of the DSM equations should be somehow removed from the results. To this end, the estimation errors of the DSM with warping-restrained elastic buckling resistances for the CFS elements under combined actions were scaled to those for the pure axial compression, as shown in Fig. 12. It should be mentioned that the average errors for combined actions and pure compression were individually obtained by taking the ratios of $(\frac{P_{DSM,W}}{P_{DFE}})$ for combined actions and pure compression, respectively. In general, it can be seen that the code suggested interaction equation was more efficient for the medium length beam-column members with an average of 4% error; however, this value reached 19% and 22% for the short and long length elements, respectively. Therefore, it can be concluded that the effects of the interaction equation are more considerable than the effects of the warping-restrained boundary conditions on the accuracy of the strength predictions. Furthermore, the results showed that the influence of the interaction equation on the total estimation error was more evident in the CFS members under combined compression and bi-axial bending moments, especially for short and medium length elements, as shown in Fig. 12.

The presented results, in general, highlight the need to develop more efficient interaction equations to design CFS beam-column elements under compression load and bending moments. Besides, more accurate methods are required to take into account the warping restrained boundary condition on the capacity predictions. This is especially important in the case CFS elements are used in moment resisting frame systems where the connections could provide warping fixity. It is also worth noting that DSM equations for long members, in which local-global buckling are determined as the dominant buckling mode, require some modifications to be more efficient.

6 Summary and conclusions

This paper assessed the accuracy of the existing methods in estimating the load-carrying capacity of CFS beam-column members as well as the effects of the warping restrained boundary condition and the efficiency of the interaction equation proposed by AISI S100 (2016) [21]. Detailed FE models were developed in ABAQUS by considering the effects of the material nonlinearity and geometric imperfections and validated against the results of two different experimental investigations on CFS lipped channel cross-sections under pure axial compression, compression and minor axis bending moment, compression and major axis bending moment, and compression and biaxial bending moments. A comprehensive parametric study was then conducted using the validated models, covering different cross-sections, lengths, and levels of load eccentricities. A total of 270 FE models were undertaken to compare their results with the current design methods in design guidelines and literature.

The accuracy of the existing design methods was compared with the detailed FE models. In general, less accurate load bearing capacity predictions were observed for short length CFS members (i.e., 500 mm) compared to the medium (i.e., 1500 mm) and long length elements (i.e., 3000 mm) under combined actions.

Compared to the other methods, the DSM provided the most conservative predictions (up to 55% lower than the detailed FE results), which can be attributed to errors associated with (i) warping restrained boundary condition effects, (ii) the DSM equations for the calculations of buckling loads, and (iii) the AISI linear interaction equation. The maximum error in DSM capacity predictions was seen when the CFS members were subjected to combined compression and bi-axial bending moments (average errors of 40%, 27% and 19% for short, medium and long length members).

The DSM with warping-restrained elastic buckling resistance (DSM,W) provided better predictions compared to the conventional DSM by up to 7.3%, while its efficiency was more evident in the shortest length elements. However, the maximum difference between the predictions of this method and the detailed FE results was still 51%.

The results of the proposed method by Moen [23] indicated a good agreement with the detailed FE models when the dominant failure mode under pure axial load was the distortional buckling mode (generally the case for short members). For these elements, this method could provide more accurate strength predictions compared to the DSM by up to 16%. However, for the other elements, the results of the DSM and the Moen's proposed method are identical.

While the method proposed by Torabian et al. [39] generally provided overestimated results compared to the detailed FE models, it led to more accurate predictions than the other design methods in most cases. A good agreement was observed with the FE models in the intermediate cross-sections (11% error on average); however, there was a considerable difference in the short specimens (25% error on average).

It was shown that considering the warping-fixed effect could on average improve the accuracy of the capacity predictions by 6%, 2.5% and 1.2% in short, medium, and long length specimens, respectively. It was demonstrated that increasing the element length reduces the effects of warping, which is attributed to the shortening of the buckling half-wavelength caused by the warping-restrained condition.

There was a noticeable estimation error (around 30% on average) between the results of the detailed FE and the current design methods based on DSM in the long CFS members under pure axial compression. The existence of such error, in the absence of interaction effect, can be referred to as the error caused by the DSM equations in which local-global buckling was determined as the dominant buckling mode.

The assessment of the interaction equation proposed by the AISI S100 (2016) [21] for the members under the combined actions of compression load and bending moments indicated the better efficiency of this method for the medium length beam-column members with an average of 4% error in the capacity predictions; however, this error increased to 19% and 22% for the short and long length elements, respectively. It can be concluded that the effects of the interaction equation on the accuracy of the strength predictions are more considerable than the warping-restrained boundary conditions. Furthermore, the results showed that the influence of the interaction equation on the total estimation error was more evident in the CFS members under combined compression and bi-axial bending moments, especially for short and medium length elements. This effect seems to be less dominant for the elements under the major axis bending moment.

Acknowledgement

The first author would like to thank the University of Auckland for providing a Doctoral Scholarship.

References

[1] Mojtabaei, Seyed Mohammad, Mohammad Zaman Kabir, Iman Hajirasouliha, and Mina Kargar. "Analytical and experimental study on the seismic performance of cold-formed steel frames." *Journal of Constructional Steel Research* 143 (2018): 18-31. https://doi.org/10.1016/j.jcsr.2017.12.013

[2] McCrum, Daniel P., Jordan Simon, Michael Grimes, Brian M. Broderick, James BP Lim, and Andrzej M. Wrzesien. "Experimental cyclic performance of cold-formed steel bolted moment resisting frames." *Engineering Structures* 181 (2019): 1-14. https://doi.org/10.1016/j.engstruct.2018.11.063

[3] Phan, Duoc T., Seyed Mohammad Mojtabaei, Iman Hajirasouliha, Jun Ye, and James BP Lim. "Coupled element and structural level optimisation framework for cold-formed steel frames." *Journal of Constructional Steel Research* 168 (2020): 105867. https://doi.org/10.1016/j.jcsr.2019.105867

[4] Mojtabaei, Seyed Mohammad, Jurgen Becque, and Iman Hajirasouliha. "Local buckling in cold-formed steel moment-resisting bolted connections: behavior, capacity, and design." *Journal of Structural Engineering* 146, no. 9 (2020): 04020167. https://doi.org/10.1061/(ASCE)ST.1943-541X.0002730

[5] Mojtabaei, Seyed Mohammad, Jurgen Becque, and Iman Hajirasouliha. "Behavior and Design of Cold-Formed Steel Bolted Connections Subjected to Combined Actions." *Journal of Structural Engineering* 147, no. 4 (2021): 04021013. https://doi.org/10.1061/(ASCE)ST.1943-541X.0002966

[6] Papargyriou, Ioannis, and Iman Hajirasouliha. "More efficient design of CFS strap-braced frames under vertical and seismic loading." *Journal of Constructional Steel Research* 185 (2021): 106886. https://doi.org/10.1016/j.jcsr.2021.106886

[7] Papargyriou, Ioannis, Iman Hajirasouliha, Jurgen Becque, and Kypros Pilakoutas. "Performance-based assessment of CFS strap-braced stud walls under seismic loading." *Journal of Constructional Steel Research* 183 (2021): 106731. https://doi.org/10.1016/j.jcsr.2021.106731

[8] Torabian, Shahabeddin, and Benjamin W. Schafer. "Development and experimental validation of the Direct Strength Method for cold-formed steel beam-columns." *Journal of Structural Engineering* 144, no. 10 (2018): 04018175. https://doi.org/10.1061/(ASCE)ST.1943-541X.0002117

[9] Torabian, Shahabeddin, Baofeng Zheng, and Benjamin W. Schafer. "Experimental response of cold-formed steel lipped channel beam-columns." *Thin-walled structures* 89 (2015): 152-168. https://doi.org/10.1016/j.tws.2014.12.003

[10] Torabian, Shahabeddin, David C. Fratamico, and Benjamin W. Schafer. "Experimental response of cold-formed steel Zee-section beam-columns." *Thin-walled structures* 98 (2016): 496-517. https://doi.org/10.1016/j.tws.2015.10.016

[11] AISI (American Iron and Steel Institute). *North American specification for the design of cold-formed steel structural members*. AISI S100-12. Washington, DC: AISI, 2012.

[12] Cheng, Shan-shan, Boksun Kim, and Long-yuan Li. "Lateral–torsional buckling of cold-formed channel sections subject to combined compression and bending." *Journal of Constructional Steel Research* 80 (2013): 174-180. https://doi.org/10.1016/j.jcsr.2012.07.026

[13] Ma, Jia-Lin, Tak-Ming Chan, and Ben Young. "Cold-formed high-strength steel rectangular and square hollow sections under combined compression and bending." *Journal of Structural Engineering* 145, no. 12 (2019): 04019154. https://doi.org/10.1061/(ASCE)ST.1943-541X.0002446

[14] ANSI/AISC (American National Standards Institute of steel Construction). *Specification for structural steel buildings*. ANSI/AISC 360-10. Chicago: AISC, 2010.

[15] CEN (European Committee for Standardization). *Eurocode 3: Design of steel structures—Part 1–1: General rules and rules for buildings*. Brussels, Belgium: CEN, 2005.

[16] AS (Australia Standards). *Standards Australia international*. New South Wales, Australia: AS, 1990.

[17] Li, Qiu-Yun, and Ben Young. "Tests of cold-formed steel built-up open section members under eccentric compressive load." *Journal of Constructional Steel Research* 184 (2021): 106775. https://doi.org/10.1016/j.jcsr.2021.106775

[18] Wang, Bin, Guillaume L. Bosco, Benoit P. Gilbert, Hong Guan, and Lip H. Teh. "Unconstrained shape optimisation of singly-symmetric and open cold-formed steel beams and beam-columns." *Thin-Walled Structures* 104 (2016): 54-61. https://doi.org/10.1016/j.tws.2016.03.007

[19] Parastesh, Hossein, Seyed Mohammad Mojtabaei, Hamed Taji, Iman Hajirasouliha, and Alireza Bagheri Sabbagh. "Constrained optimization of anti-symmetric cold-formed steel beam-column sections." *Engineering Structures* 228 (2021): 111452. https://doi.org/10.1016/j.engstruct.2020.111452

[20] Mojtabaei, Seyed Mohammad, Jurgen Becque, and Iman Hajirasouliha. "Structural Size Optimization of Single and Built-Up Cold-Formed Steel Beam-Column Members." *Journal of Structural Engineering* 147, no. 4 (2021): 04021030. https://doi.org/10.1061/(ASCE)ST.1943-541X.0002987

[21] AISI (American Iron and Steel Institute). *North American specification for the design of cold-formed steel structural members* (AISI S100-16). Washington, DC: AISI, 2016.

[22] AS/NZS 4600 (Australian Standard/New Zealand Standard)). *Cold-formed steel structures*. Sydney/Wellington, 2018.

[23] Moen, Cristopher Dennis. "*Direct strength design of cold-formed steel members with perforations*." PhD diss., Johns Hopkins University, 2009.

[24] Rajkannu, J. Sevugan, and S. Arul Jayachandran. "Flexural-torsional buckling strength of thin-walled channel sections with warping restraint." *Journal of Constructional Steel Research* 169 (2020): 106041. https://doi.org/10.1016/j.jcsr.2020.106041

[25] AISI (American Iron and Steel Institute). *Specification for the design of cold-formed steel structural members*. Washington (DC): AISI, 1996.

[26] North American Specification. *Appendix 1: Design of cold-formed steel structural members using the Direct Strength Method*. In: 2004 supplement to the north American specification for the design of cold-formed steel structures. Washington (DC): American Iron and Steel Institute, 2004.

[27] EN 1993-1-3. *Eurocode 3: Design of steel structures-Part 1-3: General rules: Supplementary rules for cold-formed members and sheeting*. Brussels: European Committee for Standardization, 2006.

[28] Schafer, Benjamin W. "The direct strength method of cold-formed steel member design." *Journal of constructional steel research* 64, no. 7-8 (2008): 766-778. https://doi.org/10.1016/j.jcsr.2008.01.022

[29] Schafer, Benjamin W., and Teoman Peköz. "Direct strength prediction of cold-formed steel members using numerical elastic buckling solutions." (1998).

[30] Fang, Zhiyuan, Krishanu Roy, Jiri Mares, Chiu-Wing Sham, Boshan Chen, and James BP Lim. "Deep learning-based axial capacity prediction for cold-formed steel channel sections using Deep Belief Network." In *Structures*, vol. 33, pp. 2792-2802. Elsevier, 2021. https://doi.org/10.1016/j.istruc.2021.05.096

[31] Ye, Jun, Seyed Mohammad Mojtabaei, and Iman Hajirasouliha. "Local-flexural interactive buckling of standard and optimised cold-formed steel columns." *Journal of constructional steel research* 144 (2018): 106-118. https://doi.org/10.1016/j.jcsr.2018.01.012

[32] Schafer, Benjamin W., CUFSM Version 5.04, Department of Civil Engineering, Johns Hopkins University, 2006. http://www.ce.jhu.edu/bschafer/cufsm/.

[33] Papangelis, J. P., & Hancock, G. J. THIN-WALL—Cross Section Analysis and Finite Strip Buckling Analysis of Thin-Walled Structures—User's Manual, 1995.

[34] Abaqus/CAE User's Manual, version 6.23, USA, (2021).

[35] Phan, Duoc T., Seyed Mohammad Mojtabaei, Iman Hajirasouliha, T. L. Lau, and James BP Lim. "Design and optimization of cold-formed steel sections in bolted moment connections considering bimoment." *Journal of Structural Engineering* 146, no. 8 (2020): 04020153. https://doi.org/10.1061/(ASCE)ST.1943-541X.0002715

[36] Ye, Jun, Jurgen Becque, Iman Hajirasouliha, Seyed Mohammad Mojtabaei, and James BP Lim. "Development of optimum cold-formed steel sections for maximum energy dissipation in uniaxial bending." *Engineering structures* 161 (2018): https://doi.org/10.1016/j.engstruct.2018.01.070

[37] Mojtabaei, Seyed Mohammad, Iman Hajirasouliha, and Jun Ye. "Optimisation of cold-formed steel beams for best seismic performance in bolted moment connections." *Journal of Constructional Steel Research* 181 (2021): 106621. https://doi.org/10.1016/j.jcsr.2021.106621

[38] Ye, Jun, Iman Hajirasouliha, and Jurgen Becque. "Experimental investigation of local-flexural interactive buckling of cold-formed steel channel columns." *Thin-walled structures* 125 (2018): 245-258. https://doi.org/10.1016/j.tws.2018.01.020

[39] Torabian, Shahabeddin, Baofeng Zheng, and B. W. Schafer. "Direct strength prediction of cold-formed steel beam-columns." *Research Rep. RP16-3. Ithaca, NY: American Iron and Steel Institute* (2016).

[40] Schafer, Benjamin W., and Teoman Peköz. "Computational modeling of cold-formed steel: characterizing geometric imperfections and residual stresses." *Journal of constructional steel research* 47, no. 3 (1998b): 193-210. https://doi.org/10.1016/S0143-974X(98)00007-8

[41] Schafer, Benjamin William, Zhan Li, and Cristopher Dennis Moen. "Computational modelling of cold-formed steel." *Thin-walled structures* 48, no. 10-11 (2010): 752-762. https://doi.org/10.1016/j.tws.2010.04.008

[42] Yu, Cheng, and Benjamin W. Schafer. "Distortional buckling tests on cold-formed steel beams." *Journal of structural engineering* 132, no. 4 (2006): 515-528. https://doi.org/10.1061/(ASCE)0733-9445(2006)132:4(515)

[43] Schafer, Benjamin W., and Teoman Peköz. "Laterally braced cold-formed steel flexural members with edge stiffened flanges." *Journal of Structural Engineering* 125, no. 2 (1999): 118-127. https://doi.org/10.1061/(ASCE)0733-9445(1999)125:2(118)

[44] MATLAB, (R2020b), MathWorks, Natick, MA, 2020.

[45] Walker, A. C. (Ed.). (1975). *Design and analysis of cold-formed sections*. John Wiley & Sons.

[46] Meza Ortiz, Francisco. "The behaviour of cold-formed steel built-up structural members." PhD diss., The University of Sheffield, 2018.

Notation

A	Cross-sectional area
A_g	Gross cross-sectional properties
b	Actual width of the plate in EWM
b_{eff}	Effective width of the plate in EWM
b_f	Flange width of a section
CDF	Cumulative distribution function
CFS	Cold formed steel
d	Depth of section
D_{boost}	Boosting factor for distortional critical buckling load
d_1	Overall depth of lip
DSM	Direct strength method
EWM	Effective width method
E	Young’s modulus of elasticity
e_x	Eccentricity in x-direction
e_y	Eccentricity in y-direction
e_z	Eccentricity in z-direction
FE	Finite element

FSM	Finite strip method
f_y	Yield strength of the material
I_1, I_2	Moment of inertia about major and minor axes, respectively
K	Effective length factor
L	Length of a member
L_e	Length of a member
L_{crd}	distortional half-wavelength
M_{crd}	Elastic distortional buckling moment
M_{cre}	Elastic lateral-torsional buckling moment
M_{crl}	Elastic local buckling moment
M_n	Nominal flexural capacity
M_{nd}	Nominal member flexural capacity for distortional buckling
M_{ne}	Nominal member flexural capacity for lateral-torsional buckling
M_{nl}	Nominal member flexural capacity for local buckling
M_x, M_y	Design bending moment around the x-and y-axes, respectively
M_{nx}, M_{ny}	Nominal member moment capacities about the x-and y-axes, respectively
M_1, M_2	Smaller and larger moment at the two ends of the member, respectively
M_{1r} , M_{2r}	Required bending moments around major and minor axis, respectively
P	Design axial force
P_{crd}	Elastic distortional buckling load
P_{cre}	Elastic global buckling stress
P_{crl}	Elastic local buckling load
P_n	Nominal capacity of a member in compression
P_{nd}	Nominal member compression capacity for distortional buckling
P_{ne}	Nominal member compression capacity for flexural, torsional and flexural-torsional buckling
P_{nl}	Nominal member compression capacity for local buckling
P_r	Required axial load
P_y	Nominal yield capacity of a member in compression
$P_{DSM,W}$	Predicted capacity from Nonlinear Elastic Buckling Analysis of ABAQUS
P_{DSM}	Predicted capacity from DSM
$P_{Distortional,W}$	Predicted capacity from Moen's method
P_{DFE}	Predicted capacity from detailed finite element models
$P_{Interaction}$	Predicted capacity from Torabian's method
P_{Test}	Experimental capacity of the reference study
P_{FE}	Maximum axial capacity of our validated FE models
t	Thickness of a channel
w_i , w_e	Warping restraint factors
w_y	Elastic section modulus

y_{c1} , y_{c2}	Distance to the centroidal principal major and minor axes, respectively
Z_y	Elastic section modulus
β	Radial length
θ_{MM}	Azimuth angle
λ_c	Non-dimensional slenderness used to determine P_{ne}
λ_d	Non-dimensional slenderness used to determine P_{nd} and M_{nd}
λ_l	Non-dimensional slenderness used to determine P_{nl} and M_{nl}
λ_s	Cross-sectional slenderness
$\emptyset_{PM}$	Elevation angle,
ε_e	Measured engineering strain
ε_{true}	True strain
σ_{cr}	Elastic critical local/distortional buckling stress
σ_e	Measured engineering stress
σ_r	Required axial stress
σ_{true}	True stress
$\sigma_{0.2\%}$	Proof stress of the material

List of Tables

Table. 1 Comparison between the strength of CFS elements under pure axial compression obtained from the FE models (P^{FE}) and tests (P^{Test}) [38]

Specimen	Length (mm)	P_{Test} (kN)	P_{FE} (kN)	P_{Test}/P_{FE}
A1000-a	1000	99.8	103.8	0.96
A2000-a	2000	78.4	74.8	1.05
B1000-b	1000	110.3	113.1	0.98
B1500-c	1500.1	106.2	108.8	0.98
C1000-c	999.8	42.7	46.2	0.92
C1500-b	1500.1	35.2	34.1	1.03
D1000-a	1000	109	101.8	1.07
D1500-a	1500	95	90.7	1.05
Average				1.005
Standard deviation				0.05

Table. 2 Comparison between the strength of CFS elements under combined action of axial compression and bending moment obtained from the FE models (P^{FE}) and tests (P^{Test}) [39]

Section name	e_y (mm)	e_x (mm)	P_{Test} (kN)	P_{FE} (kN)	P_{Test}/P_{FE}
S600-305-1	0	-25.4	25.4	25.5	1.00
S600-305-11	-191	0	20.6	20.2	1.02
S600-305-15	-76.2	15.24	25.0	26.1	0.96
S600-610-5	0	15.24	25.0	24.6	1.02
S600-610-8	-76.2	0	34.8	35.5	0.98
S600-610-15	-69.9	-14.2	25.0	25.4	0.98
S600-1219-1	0	-38.1	11.1	11.3	0.98
S600-1219-9	-140	0	23.4	23.0	1.02
S600-1219-15	-63.5	-13	17.6	17.4	1.01
Average					1.00
Standard deviation					0.02

Table. 3 Parametric study variables

Section name	Web (d) (mm)	Flange (b_f) (mm)	Lip (d_1) (mm)	Thickness (t) (mm)	Length (L) (mm)
$C1$	300	50	25	1	500
				2	1500
				4	3000
$C2$	250	75	25	1	500
				2	1500
				4	3000
$C3$	200	100	25	1	500
				2	1500
				4	3000

Table. 4 Magnitude of eccentricities

Loading condition	e_y (mm)	e_x (mm)
Pure compression	0	0
Minor axis bending + compression load	0	10
	0	-25
	0	50
Major axis bending + compression load	10	0
	100	0
	200	0
Bi-axial bending moment + compression load	10	10
	100	-25
	200	50

*Negative sign shows that the lips of the specimens are in tension.

Table. 5 Dominant failure mode of selected cross-sections under pure actions

Cross-section	Length (mm)	Thickness (mm)	Dominant failure modes of cross-sections based on DSM results			
			Compression	**Major axis bending**	**Minor axis bending (web in compression)**	**Minor axis bending (web in tension)**
$C1$	500	1	Distortional	Local	Yield	Local
		2	Distortional	Local	Yield	Yield
		4	Distortional	Yield	Yield	Yield
	1500	1	Local	Local	Yield	Local
		2	Local	Distortional	Yield	Yield
		4	Local	Local	Yield	Yield
	3000	1	Local	Local	Yield	Local
		2	Local	Local	Yield	Local
		4	Local-Global	Local	Yield	Local & Global
$C2$	500	1	Local	Local	Yield	Distortional
		2	Local	Distortional	Yield	Distortional
		4	Distortional	Yield	Yield	Yield
	1500	1	Local	Local	Yield	Distortional
		2	Local	Distortional	Yield	Distortional
		4	Local	Yield	Yield	Yield
	3000	1	Local	Local	Yield	Distortional
		2	Local	Local	Yield	Distortional
		4	Local-Global	Local	Yield	Local & Global
$C3$	500	1	Local	Local	Yield	Distortional
		2	Local	Distortional	Local	Distortional
		4	Distortional	Distortional	Yield	Yield
	1500	1	Local	Local	Yield	Distortional
		2	Local	Distortional	Local	Distortional
		4	Local	Distortional	Yield	Yield
	3000	1	Local	Local	Yield	Distortional
		2	Local	Distortional	Local	Distortional
		4	Local-Global	Local	Yield	Local & Global

List of Figures

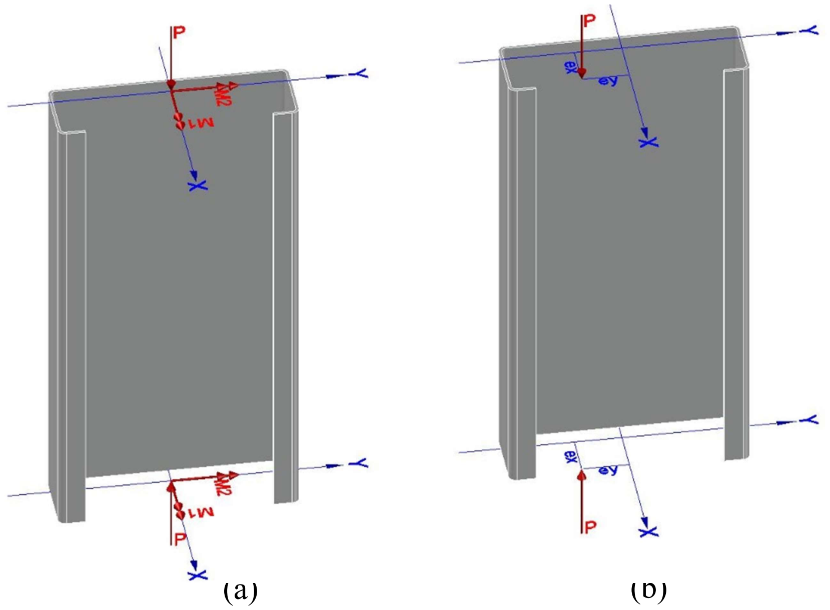

Fig. 1 Beam-column members subjected to (a) combined axial load and bending moment (b) eccentric axial load

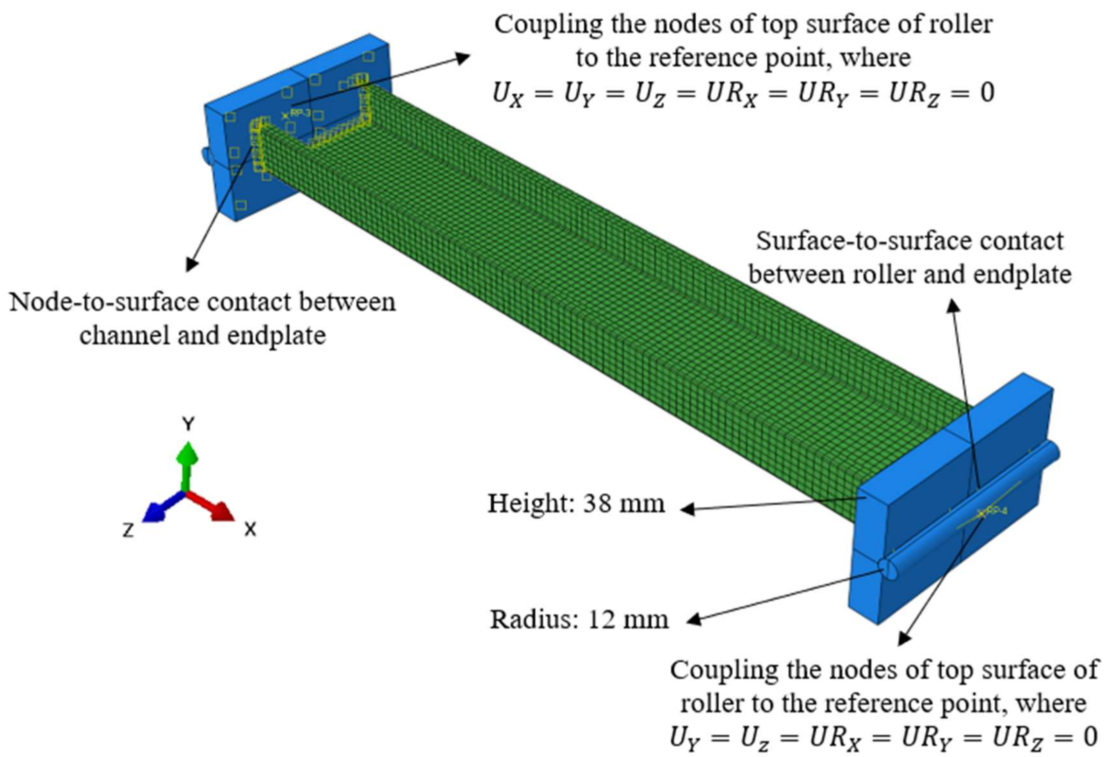

Fig. 2 Boundary conditions of CFS elements under pure axial compressive loads (adopted from Ye et al. [38])

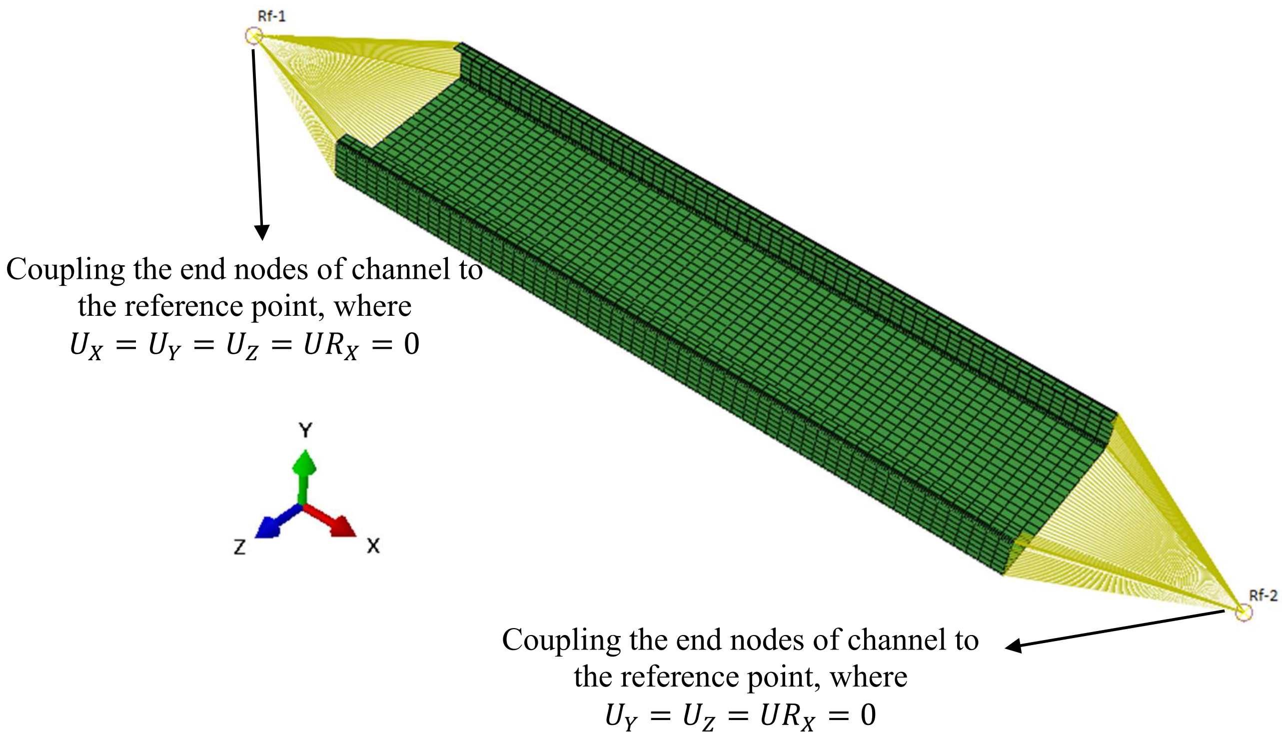

Fig. 3 Boundary conditions of CFS elements under eccentric compressive loads (adopted from Torabian et al. [39])

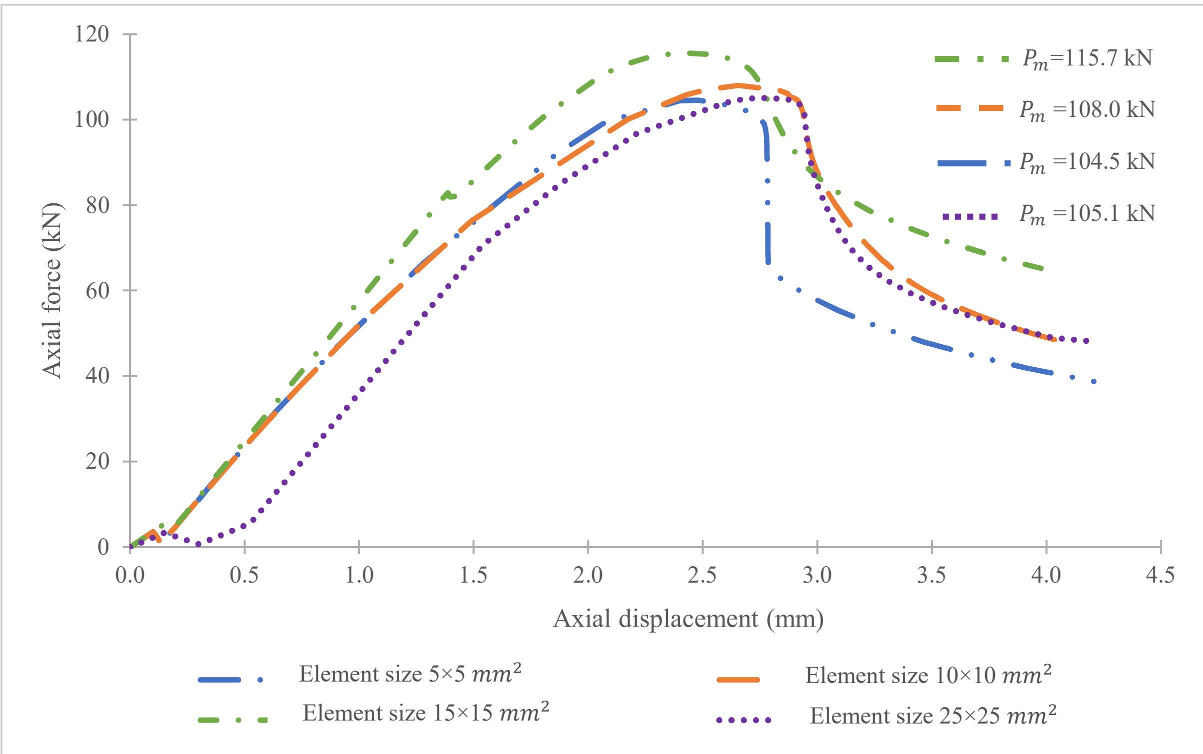

Fig. 4 Axial load vs displacement of B1500-c specimen with various element sizes in flat regions and the number of four elements in corners

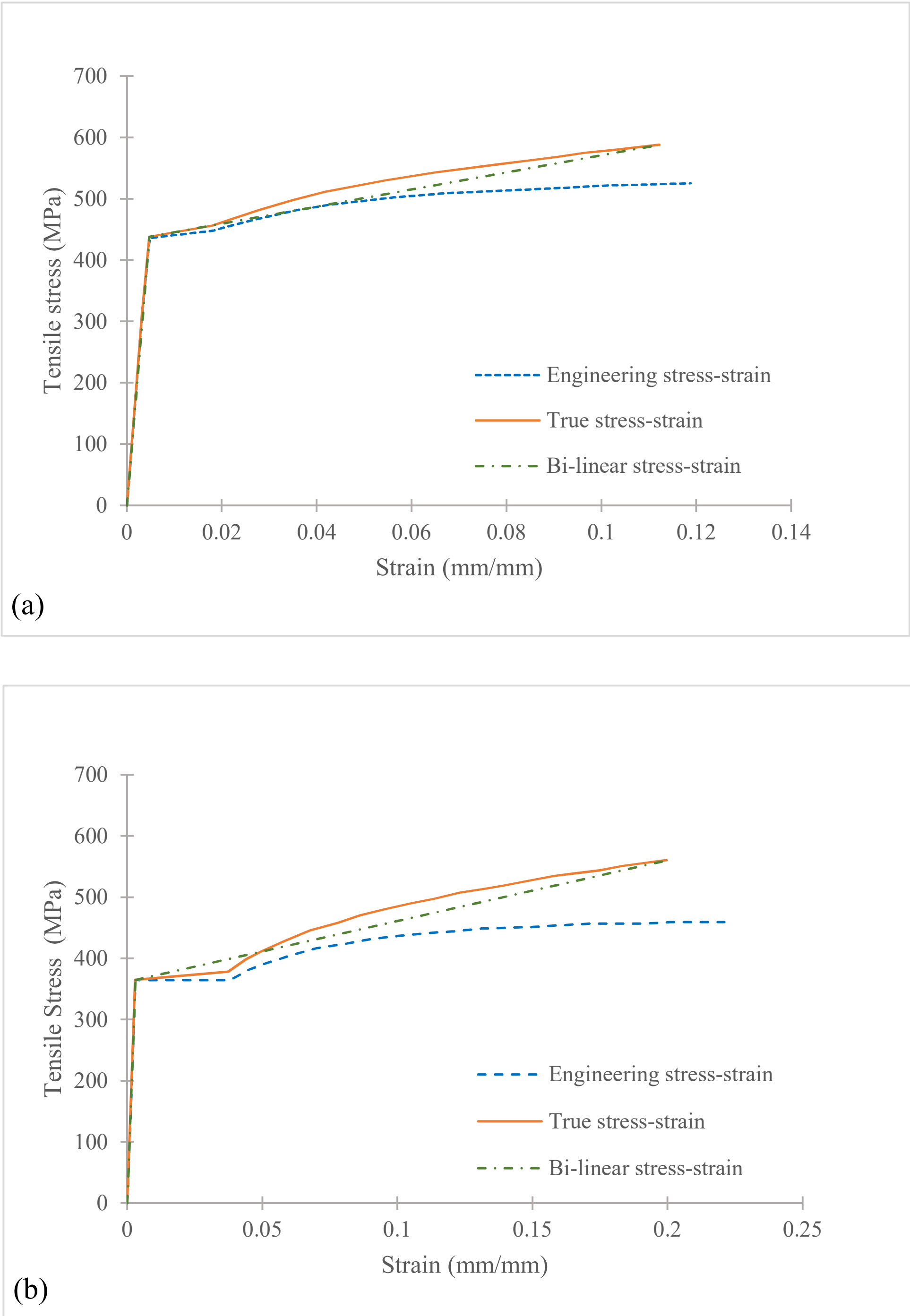

Fig. 5 Stress-strain curves for: (a) columns (Ye et al. [38]) and (b) beam-columns (Torabian et al. [39])

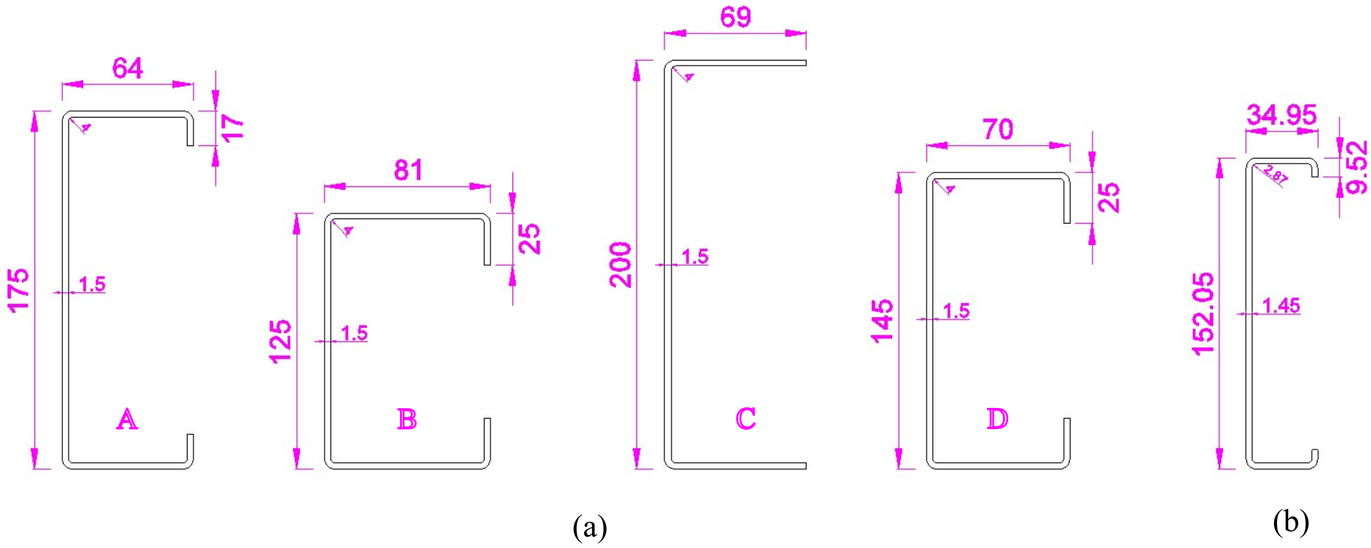

Fig. 6 Cross-sectional geometry of the tested: (a) columns [38] and (b) beam-columns [39]

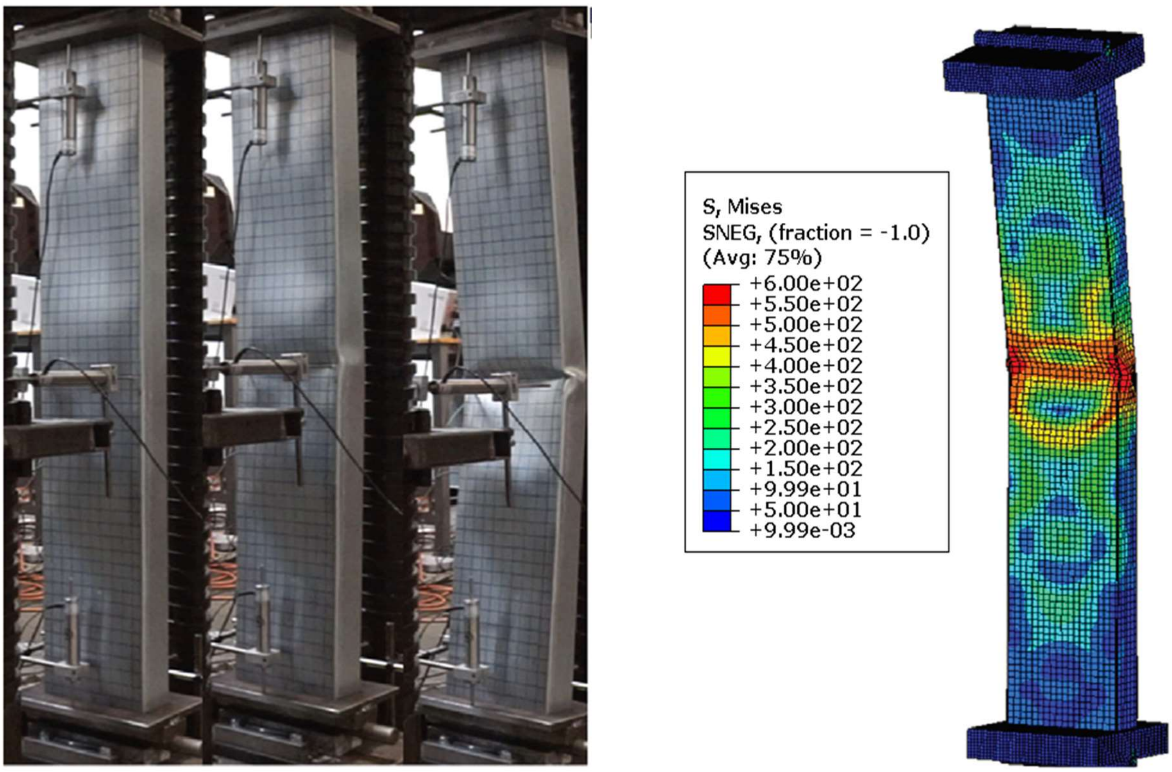

Fig. 7 Failure mode obtained from FE model vs experimental result (A1000-a) (test set-up adopted from Ye et al. [38])

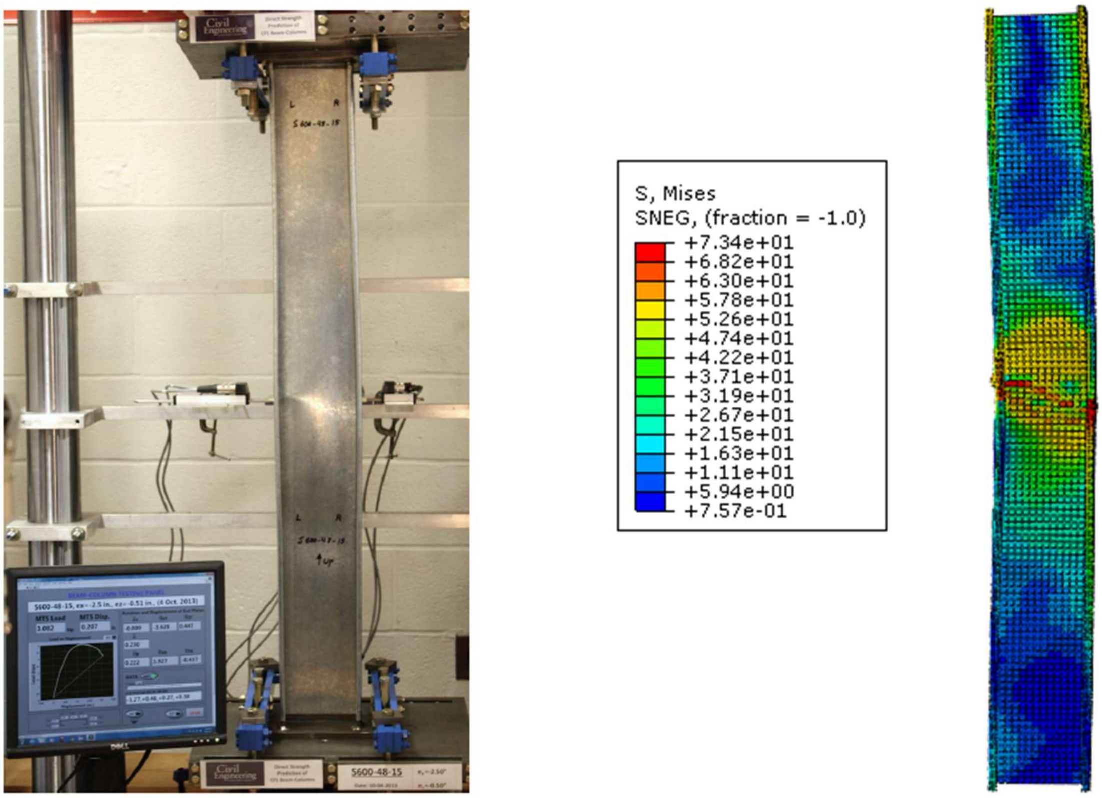

Fig. 8 Failure mode obtained from FE model vs experimental result (S600-1219-15) (test set-up adopted from Torabian et al. [39])

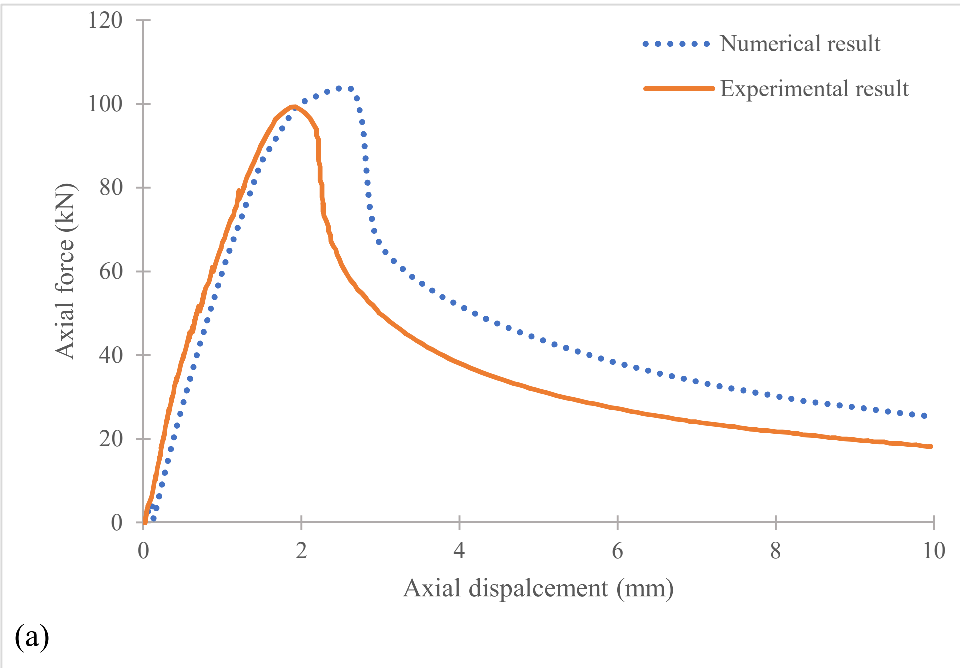

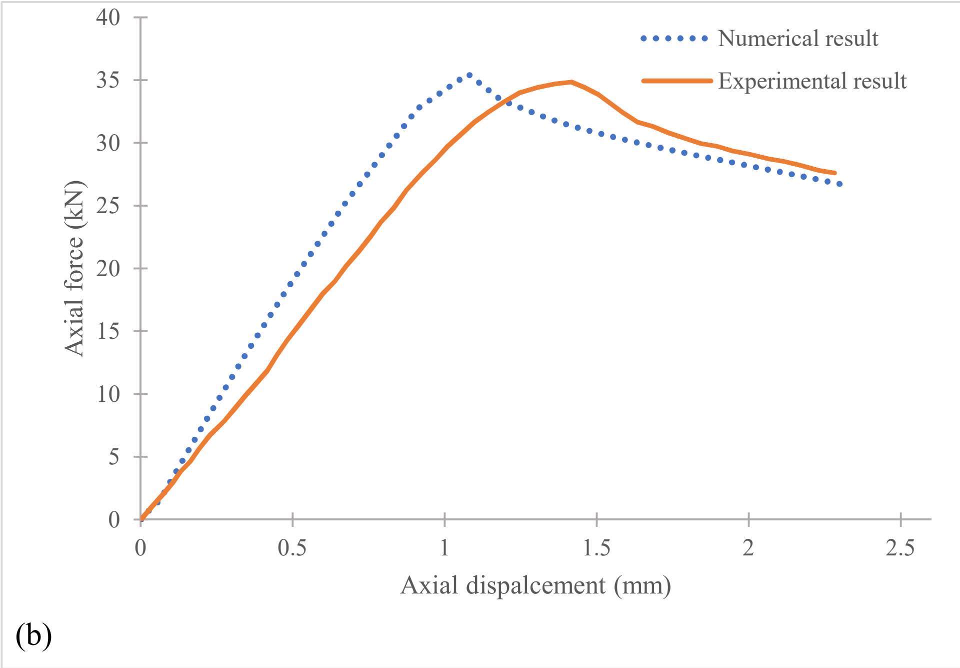

Fig. 9 Axial force-displacement relationship resulting from reference experimental tests against FE (a) A1000-a and (b) S600-610-8

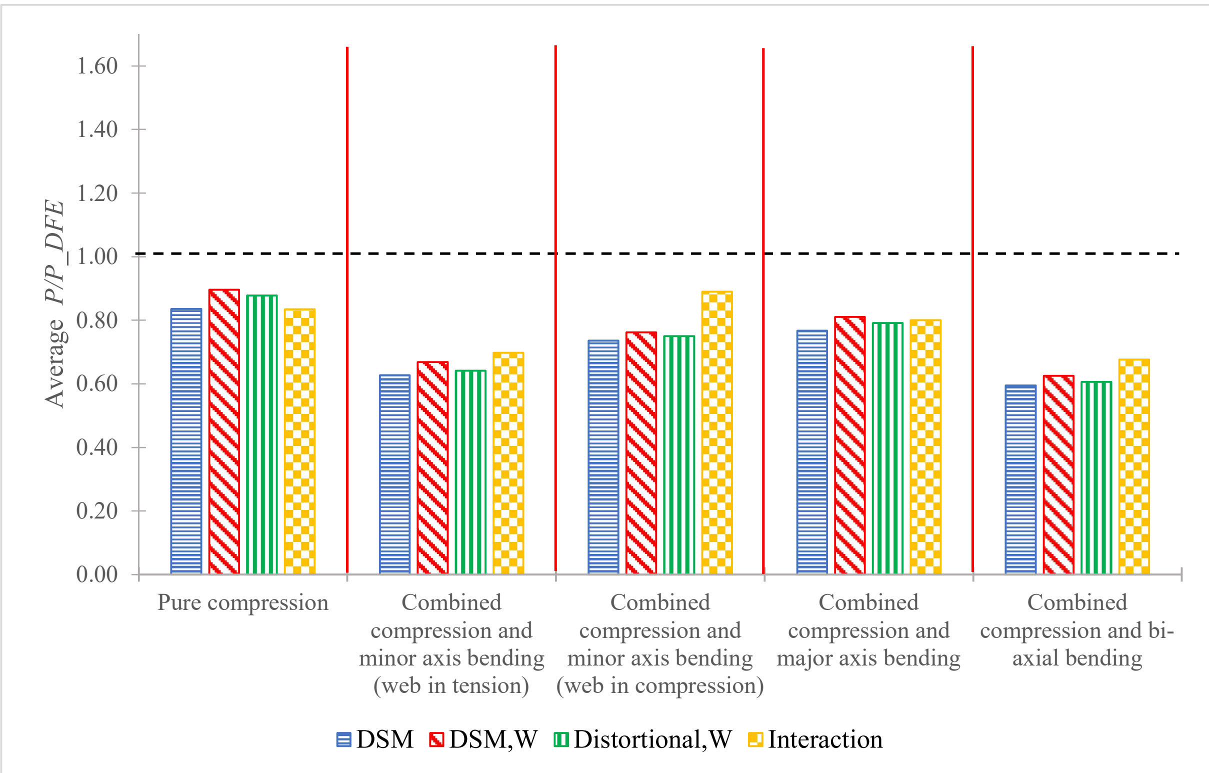

(a) 500 mm

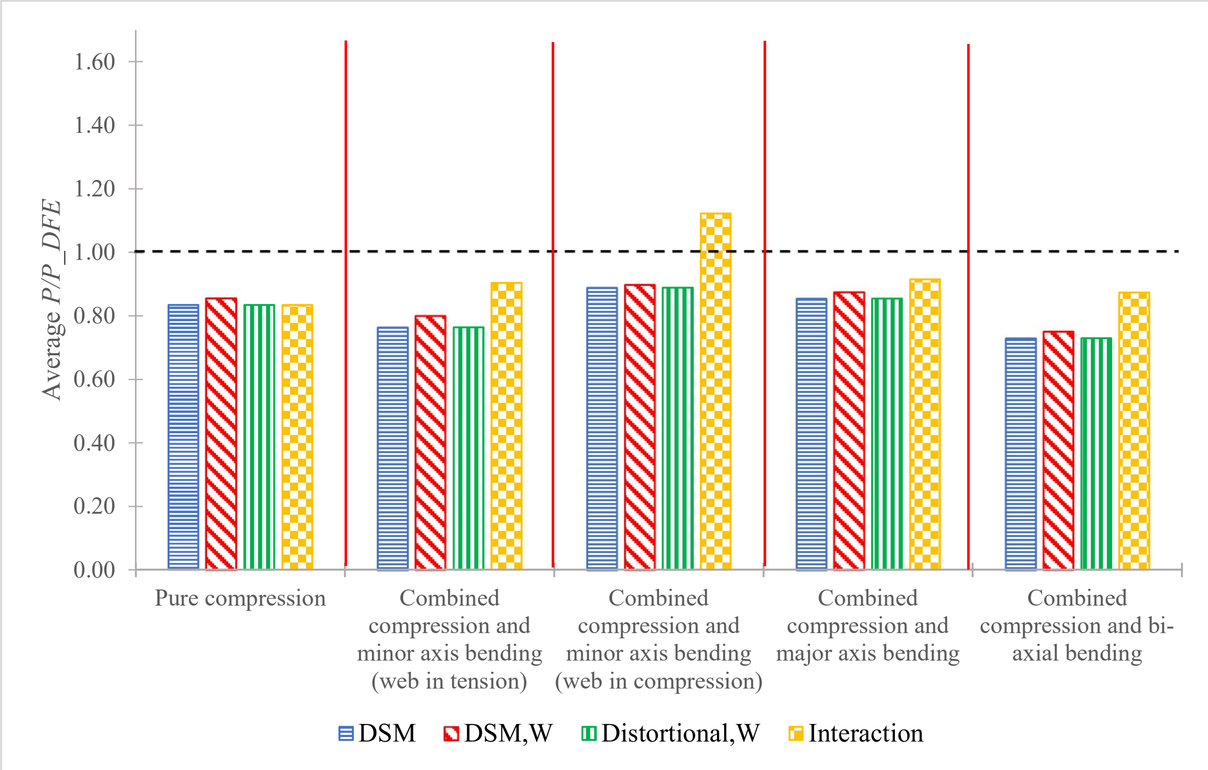

(b) 1500 mm

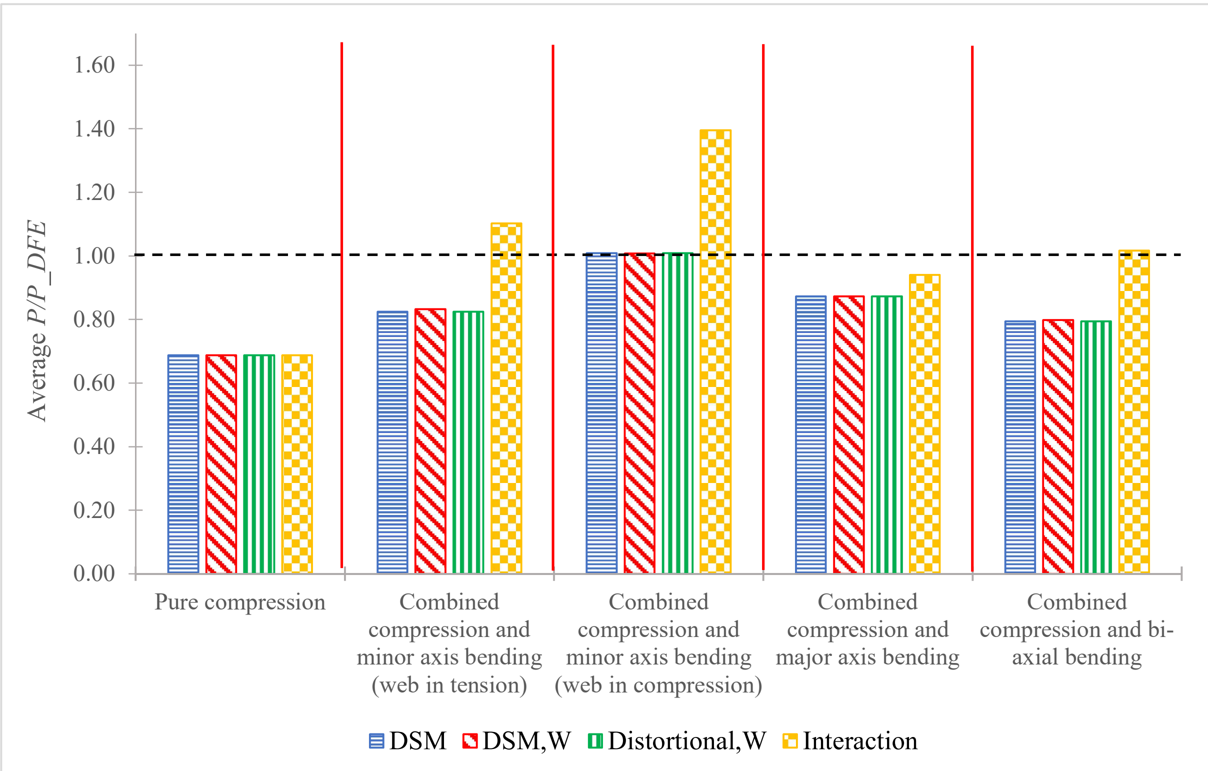

(c) 3000 mm

Fig. 10 Average ratios associated with the existing design methods in comparison with the detailed FE models for the strength calculations of CFS elements under various loading conditions

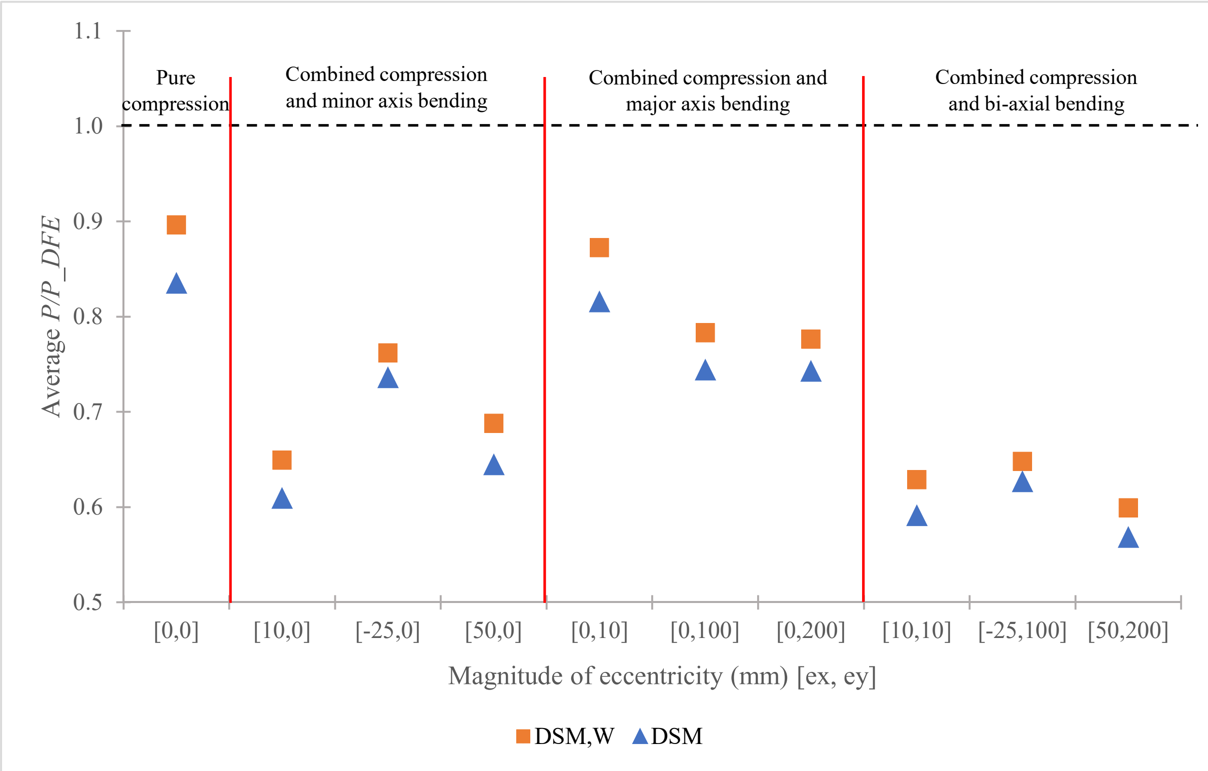

(a) 500 mm

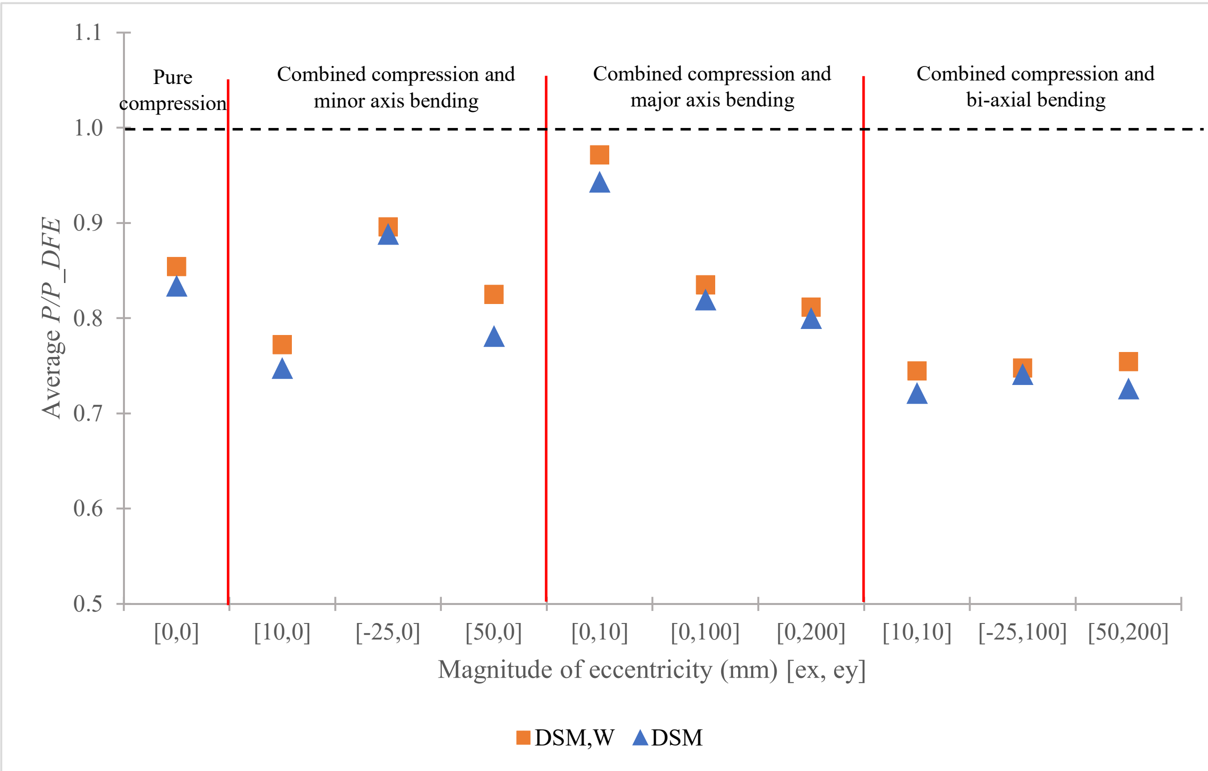

(b) 1500 mm

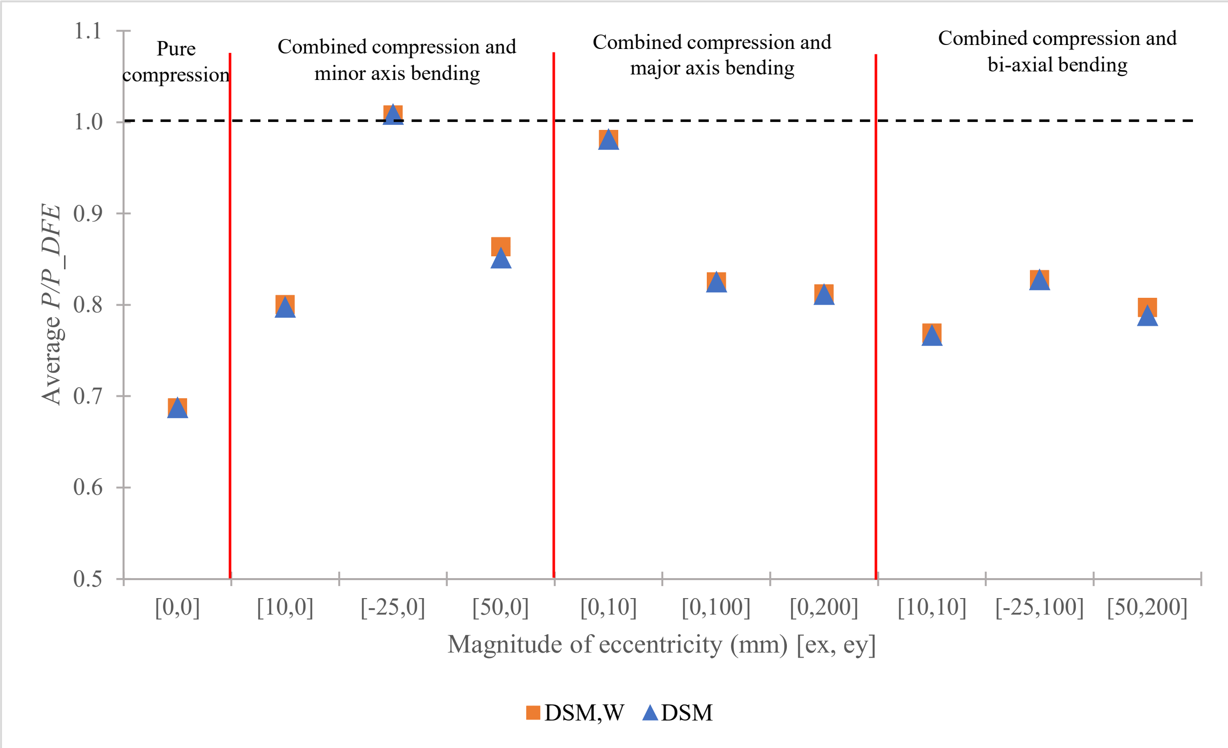

(c) 3000 mm

Fig. 11 Average ratios associated with the DSM and DSM with warping-restrained elastic buckling resistance in comparison to the detailed FE models for the CFS elements under various eccentricity values

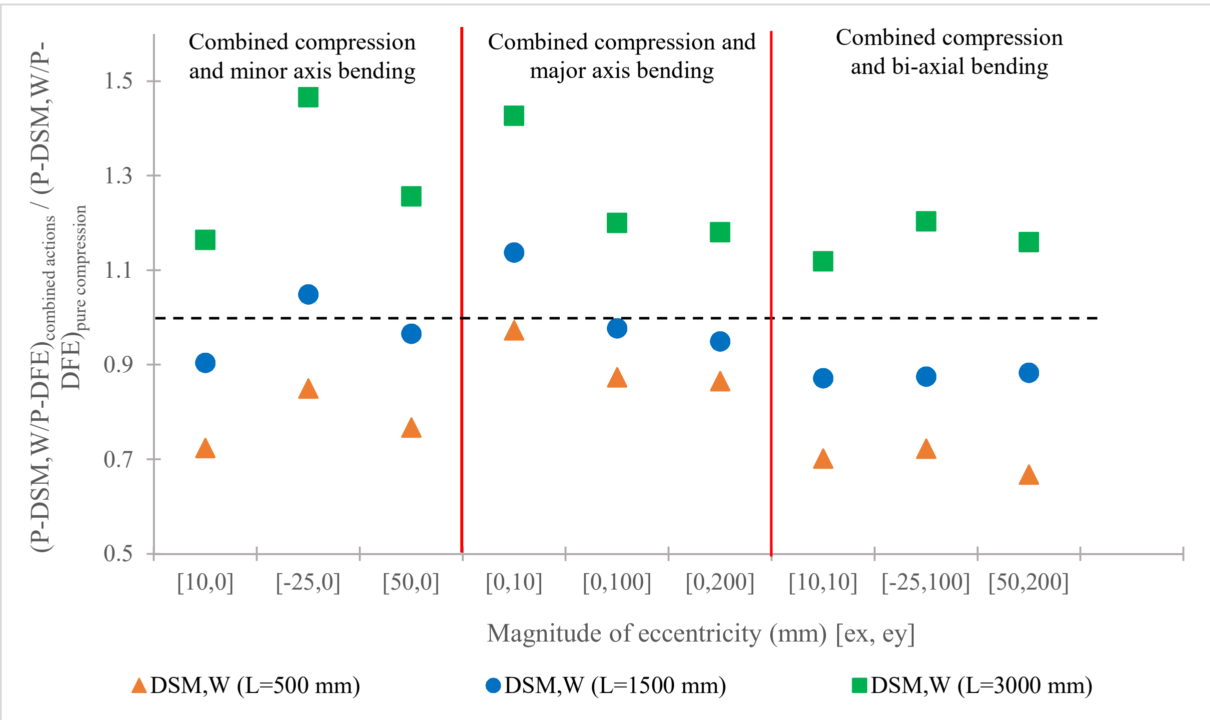

Fig. 12 Average errors associated with the DSM with warping-restrained elastic buckling resistances for the CFS elements under combined actions scaled to those under pure compression

Appendix A

Table. A1 Comparison between the results of strength for the beam-column members with $C1$ cross-section (d = 300 mm, b_f = 50 mm, d_1 = 25 mm) obtained from detailed FE models and different design methods.

Length	**Thickness**	**Eccentricity**		**Capacity**					**Ratio of each design method prediction to the detailed FE result**			
L (mm)	**t (mm)**	e_y **(mm)**	e_x **(mm)**	P_{DFE} **(kN)**	P_{DSM} **(kN)**	$P_{DSM,W}$ **(kN)**	$P_{Distortional,W}$ **(kN)**	$P_{Interaction}$ **(kN)**	$\frac{P_{DSM}}{P_{DFE}}$	$\frac{P_{DSM,W}}{P_{DFE}}$	$\frac{P_{Distortional,W}}{P_{DFE}}$	$\frac{P_{Interaction}}{P_{DFE}}$
500	1	0	0	47.9	36.4	40.5	38.2	36.4	0.76	0.85	0.80	0.76
		0	10	58.2	26.8	29.0	27.7	28.0	0.46	0.50	0.48	0.48
		0	-25	25.0	21.3	22.7	21.9	21.6	0.86	0.91	0.88	0.86
		0	50	17.6	13.0	13.6	13.2	17.4	0.74	0.77	0.75	0.99
		10	0	43.1	34.4	38.0	35.9	35.5	0.80	0.88	0.83	0.82
		100	0	33.5	22.8	24.3	23.4	23.4	0.68	0.73	0.70	0.70
		200	0	25.1	16.6	17.4	16.9	17.0	0.66	0.69	0.67	0.68
		10	10	56.6	25.6	27.7	26.5	27.1	0.45	0.49	0.47	0.48
		100	-25	22.6	15.8	16.5	16.1	15.5	0.70	0.73	0.71	0.69
		200	50	15.7	9.1	9.4	9.2	12.7	0.58	0.60	0.59	0.81
			Average	**34.51**	**22.18**	**23.91**	**22.91**	**23.46**	**0.67**	**0.71**	**0.69**	**0.73**
			Standard deviation	**15.86**	**8.91**	**10.15**	**9.45**	**8.22**	**0.14**	**0.15**	**0.14**	**0.16**
500	2	0	0	149.6	110.2	123.4	127.3	110.2	0.74	0.82	0.85	0.74
		0	10	141.5	75.6	81.6	83.3	86.2	0.53	0.58	0.59	0.61
		0	-25	76.2	51.4	54.1	54.9	65.1	0.68	0.71	0.72	0.85
		0	50	54.3	33.5	34.7	35.0	41.7	0.62	0.64	0.64	0.77
		10	0	139.1	104.2	116.0	119.4	106.0	0.75	0.83	0.86	0.76
		100	0	106.5	70.2	75.4	76.8	77.0	0.66	0.71	0.72	0.72
		200	0	78.1	51.5	54.3	55.0	55.4	0.66	0.69	0.70	0.71
		10	10	141.1	72.8	78.3	79.9	83.5	0.52	0.56	0.57	0.59

		100	-25	69.1	40.6	42.3	42.7	51.1	0.59	0.61	0.62	0.74
		200	50	48.8	24.9	25.5	25.7	31.1	0.51	0.52	0.53	0.64
			Average	**100.43**	**63.50**	**68.56**	**69.98**	**70.73**	**0.62**	**0.67**	**0.68**	**0.71**
			Standard deviation	**39.65**	**28.51**	**32.78**	**34.04**	**26.47**	**0.09**	**0.11**	**0.11**	**0.08**
500	4	0	0	426.0	347.3	381.2	405.1	347.3	0.82	0.89	0.95	0.82
		0	10	283.0	190.3	200.0	206.4	230.0	0.67	0.71	0.73	0.81
		0	-25	188.0	113.4	116.7	118.9	223.7	0.60	0.62	0.63	1.19
		0	50	103.3	67.7	68.9	69.7	73.9	0.66	0.67	0.67	0.72
		10	0	392.0	323.4	352.6	372.9	328.3	0.83	0.90	0.95	0.84
		100	0	279.8	199.7	210.5	217.6	216.3	0.71	0.75	0.78	0.77
		200	0	200.0	140.2	145.4	148.7	152.1	0.70	0.73	0.74	0.76
		10	10	282.8	182.9	191.8	197.7	220.2	0.65	0.68	0.70	0.78
		100	-25	168.6	91.3	93.5	94.9	138.1	0.54	0.55	0.56	0.82
		200	50	98.1	52.6	53.3	53.7	56.2	0.54	0.54	0.55	0.57
			Average	**242.14**	**170.87**	**181.40**	**188.55**	**198.61**	**0.67**	**0.70**	**0.73**	**0.81**
			Standard deviation	**111.13**	**100.54**	**111.96**	**120.02**	**96.01**	**0.10**	**0.12**	**0.14**	**0.15**
1500	1	0	0	34.4	29.0	29.4	29.0	29.0	0.84	0.85	0.84	0.84
		0	10	41.5	22.5	23.9	22.5	26.5	0.54	0.58	0.54	0.64
		0	-25	17.9	18.6	18.7	18.6	19.4	1.04	1.04	1.04	1.08
		0	50	16.5	11.9	13.7	11.9	17.4	0.72	0.83	0.72	1.05
		10	0	28.5	27.6	28.0	27.6	28.5	0.97	0.98	0.97	1.00
		100	0	24.9	19.4	19.5	19.4	20.7	0.78	0.79	0.78	0.83
		200	0	20.4	14.6	14.6	14.6	15.4	0.72	0.72	0.72	0.76
		10	10	40.9	21.7	23.0	21.7	25.6	0.53	0.56	0.53	0.63
		100	-25	16.5	14.1	14.2	14.1	14.9	0.85	0.86	0.85	0.90
		200	50	12.6	8.5	9.3	8.5	12.7	0.67	0.74	0.67	1.01
			Average	**25.40**	**18.79**	**19.44**	**18.79**	**21.01**	**0.77**	**0.80**	**0.77**	**0.87**
			Standard deviation	**10.50**	**6.66**	**6.59**	**6.66**	**6.01**	**0.17**	**0.16**	**0.17**	**0.16**
1500	2	0	0	110.1	94.8	95.7	94.8	94.8	0.86	0.87	0.86	0.86
		0	10	86.9	68.0	68.5	68.0	85.0	0.78	0.79	0.78	0.98

		0	-25	49.1	47.8	48.0	47.8	66.8	0.97	0.98	0.97	1.36
		0	50	37.7	32.0	32.1	32.0	41.7	0.85	0.85	0.85	1.10
		10	0	82.9	90.2	91.0	90.2	92.4	1.09	1.10	1.09	1.11
		100	0	72.9	62.7	63.1	62.7	67.2	0.86	0.87	0.86	0.92
		200	0	59.5	46.9	47.0	46.9	49.8	0.79	0.79	0.79	0.84
		10	10	86.7	65.6	66.1	65.6	82.2	0.76	0.76	0.76	0.95
		100	-25	45.9	38.0	38.1	38.0	46.2	0.83	0.83	0.83	1.01
		200	50	33.3	23.8	23.8	23.8	31.1	0.71	0.71	0.71	0.93
Average				**66.50**	**56.97**	**57.35**	**56.97**	**65.71**	**0.85**	**0.85**	**0.85**	**1.01**
Standard deviation				**25.24**	**23.65**	**23.96**	**23.65**	**22.65**	**0.11**	**0.11**	**0.11**	**0.15**
1500	4	0	0	336.5	288.0	344.7	288.0	288.0	0.86	1.02	0.86	0.86
		0	10	160.8	171.0	189.4	171.0	226.3	1.06	1.18	1.06	1.41
		0	-25	110.5	106.2	113.1	106.2	177.9	0.96	1.02	0.96	1.61
		0	50	71.5	65.1	67.6	65.1	73.8	0.91	0.95	0.91	1.03
		10	0	209.7	270.2	319.5	270.2	281.6	1.29	1.52	1.29	1.34
		100	0	186.2	173.7	192.8	173.7	203.4	0.93	1.04	0.93	1.09
		200	0	152.2	124.3	133.8	124.3	141.3	0.82	0.88	0.82	0.93
		10	10	160.6	164.5	181.6	164.5	221.8	1.02	1.13	1.02	1.38
		100	-25	105.6	85.5	89.9	85.5	133.5	0.81	0.85	0.81	1.26
		200	50	64.2	50.2	51.7	50.2	55.6	0.78	0.80	0.78	0.87
Average				**155.77**	**149.87**	**168.40**	**149.87**	**180.32**	**0.94**	**1.04**	**0.94**	**1.18**
Standard deviation				**79.32**	**80.70**	**99.62**	**80.70**	**79.46**	**0.15**	**0.21**	**0.15**	**0.26**
3000	1	0	0	18.0	13.7	13.8	13.7	13.7	0.76	0.77	0.76	0.76
		0	10	20.5	12.0	12.0	12.0	17.0	0.58	0.59	0.58	0.83
		0	-25	10.2	10.8	10.9	10.8	11.9	1.06	1.07	1.06	1.16
		0	50	10.8	7.9	7.9	7.9	14.5	0.73	0.73	0.73	1.34
		10	0	13.9	13.2	13.3	13.2	13.7	0.96	0.96	0.96	0.99
		100	0	13.1	10.1	10.1	10.1	10.7	0.77	0.77	0.77	0.82
		200	0	11.7	7.9	7.9	7.9	8.2	0.68	0.68	0.68	0.70
		10	10	20.7	11.6	11.7	11.6	16.6	0.56	0.56	0.56	0.80

		100	-25	9.7	8.4	8.4	8.4	9.4	0.87	0.87	0.87	0.97
		200	50	8.6	5.5	5.6	5.5	9.9	0.64	0.64	0.64	1.15
			Average	**13.72**	**10.12**	**10.16**	**10.12**	**12.57**	**0.76**	**0.76**	**0.76**	**0.95**
			Standard deviation	**4.46**	**2.64**	**2.66**	**2.64**	**3.02**	**0.16**	**0.16**	**0.16**	**0.21**
3000	2	0	0	61.8	43.0	43.1	43.0	43.0	0.69	0.70	0.69	0.70
		0	10	40.4	35.8	35.9	35.8	52.9	0.89	0.89	0.89	1.31
		0	-25	25.8	29.7	29.8	29.7	37.8	1.15	1.16	1.15	1.47
		0	50	22.8	21.4	21.4	21.4	32.5	0.94	0.94	0.94	1.42
		10	0	35.8	41.4	41.5	41.4	43.1	1.16	1.16	1.16	1.20
		100	0	34.0	31.2	31.3	31.2	33.8	0.92	0.92	0.92	0.99
		200	0	30.1	24.5	24.5	24.5	25.6	0.81	0.82	0.81	0.85
		10	10	40.2	34.7	34.8	34.7	51.9	0.86	0.86	0.86	1.29
		100	-25	24.8	23.6	23.6	23.6	21.2	0.95	0.95	0.95	0.85
		200	50	19.2	15.6	15.6	15.6	21.0	0.81	0.81	0.81	1.09
			Average	**33.50**	**30.07**	**30.16**	**30.07**	**36.26**	**0.92**	**0.92**	**0.92**	**1.12**
			Standard deviation	**12.32**	**8.88**	**8.92**	**8.88**	**11.59**	**0.15**	**0.15**	**0.15**	**0.26**
3000	4	0	0	153.3	96.2	96.2	96.2	96.2	0.63	0.63	0.63	0.63
		0	10	72.8	77.2	77.2	77.2	107.2	1.06	1.06	1.06	1.47
		0	-25	53.5	61.2	61.2	61.2	109.1	1.14	1.14	1.14	2.04
		0	50	42.7	43.1	43.1	43.1	61.9	1.01	1.01	1.01	1.45
		10	0	77.0	92.3	92.3	92.3	97.3	1.20	1.20	1.20	1.26
		100	0	73.1	67.4	67.4	67.4	74.7	0.92	0.92	0.92	1.02
		200	0	64.9	51.9	51.9	51.9	53.3	0.80	0.80	0.80	0.82
		10	10	72.6	74.7	74.7	74.7	106.2	1.03	1.03	1.03	1.46
		100	-25	52.1	48.1	48.1	48.1	82.1	0.92	0.92	0.92	1.58
		200	50	35.8	31.2	31.2	31.2	40.6	0.87	0.87	0.87	1.13
			Average	**69.78**	**64.34**	**64.34**	**64.34**	**82.86**	**0.96**	**0.96**	**0.96**	**1.29**
			Standard deviation	**32.57**	**21.23**	**21.23**	**21.23**	**24.44**	**0.17**	**0.17**	**0.17**	**0.41**
			Average of all 90 results	**82.42**	**65.19**	**69.30**	**67.96**	**76.84**	**0.80**	**0.82**	**0.81**	**0.96**
			Standard deviation of all 90 results	**36.78**	**31.30**	**35.32**	**34.14**	**30.87**	**0.14**	**0.15**	**0.14**	**0.21**

Table. A2 Comparison between the results of strength for the beam-column members with $C2$ cross-section (d = 300 mm, b_f = 50 mm, d_1 = 25 mm) obtained from detailed FE models and different design methods.

Length	**Thickness**	**Eccentricity**		**Capacity**					**Ratio of each design method prediction to the detailed FE result**			
L (mm)	**t (mm)**	e_y **(mm)**	e_x **(mm)**	P_{DFE} (kN)	P_{DSM} (kN)	$P_{DSM,W}$ (kN)	$P_{Distortional,W}$ (kN)	$P_{Interaction}$ (kN)	$\frac{P_{DSM}}{P_{DFE}}$	$\frac{P_{DSM,W}}{P_{DFE}}$	$\frac{P_{Distortional,W}}{P_{DFE}}$	$\frac{P_{Interaction}}{P_{DFE}}$
500	1	0	0	52.0	43.8	46.2	43.8	43.8	0.84	0.89	0.84	0.84
		0	10	60.8	34.4	36.5	34.4	35.7	0.57	0.60	0.57	0.59
		0	-25	33.5	29.5	30.6	29.5	26.8	0.88	0.91	0.88	0.80
		0	50	26.5	18.4	19.9	18.4	22.0	0.70	0.75	0.70	0.83
		10	0	49.5	41.0	43.1	41.0	40.7	0.83	0.87	0.83	0.82
		100	0	33.1	26.0	26.9	26.0	25.7	0.79	0.81	0.79	0.78
		200	0	22.8	18.5	18.9	18.5	18.6	0.81	0.83	0.81	0.81
		10	10	57.3	32.6	34.5	32.6	34.1	0.57	0.60	0.57	0.59
		100	-25	26.5	20.2	20.7	20.2	18.5	0.76	0.78	0.76	0.70
		200	50	18.7	11.7	12.3	11.7	14.3	0.63	0.66	0.63	0.77
Average				**38.06**	**27.63**	**28.96**	**27.63**	**28.03**	**0.74**	**0.77**	**0.74**	**0.75**
Standard deviation				**15.40**	**10.51**	**11.16**	**10.51**	**10.09**	**0.12**	**0.12**	**0.12**	**0.10**
500	2	0	0	185.5	146.2	153.8	146.2	146.2	0.79	0.83	0.79	0.79
		0	10	205.2	106.7	113.3	106.7	116.3	0.52	0.55	0.52	0.57
		0	-25	109.5	79.1	81.3	79.1	88.3	0.72	0.74	0.72	0.81
		0	50	91.1	51.3	55.2	51.3	56.9	0.56	0.61	0.56	0.62
		10	0	172.4	135.7	143.0	135.7	135.3	0.79	0.83	0.79	0.78
		100	0	120.0	82.6	87.6	82.6	84.3	0.69	0.73	0.69	0.70
		200	0	82.9	57.5	61.3	57.5	60.3	0.69	0.74	0.69	0.73
		10	10	202.6	101.0	107.3	101.0	110.7	0.50	0.53	0.50	0.55
		100	-25	94.0	55.8	58.1	55.8	60.4	0.59	0.62	0.59	0.64
		200	50	65.3	33.3	35.8	33.3	36.8	0.51	0.55	0.51	0.56
Average				**132.83**	**84.93**	**89.66**	**84.93**	**89.53**	**0.64**	**0.67**	**0.64**	**0.68**

Standard deviation				**53.18**	**37.26**	**39.14**	**37.26**	**36.59**	**0.11**	**0.12**	**0.11**	**0.10**
500	4	0	0	502.8	456.6	509.5	467.0	456.6	0.91	1.01	0.93	0.91
		0	10	408.2	288.1	308.3	292.2	316.0	0.71	0.76	0.72	0.77
		0	-25	298.9	185.5	193.6	187.1	274.6	0.62	0.65	0.63	0.92
		0	50	182.0	116.4	119.5	117.0	122.9	0.64	0.66	0.64	0.68
		10	0	485.3	414.0	457.0	422.5	423.7	0.85	0.94	0.87	0.87
		100	0	296.7	225.1	237.2	227.5	244.8	0.76	0.80	0.77	0.82
		200	0	198.7	149.3	154.6	150.4	162.3	0.75	0.78	0.76	0.82
		10	10	406.8	270.6	288.3	274.1	300.3	0.67	0.71	0.67	0.74
		100	-25	249.9	130.8	134.8	131.6	184.5	0.52	0.54	0.53	0.74
		200	50	146.5	76.3	77.7	76.6	79.6	0.52	0.53	0.52	0.54
Average				**317.57**	**231.27**	**248.05**	**234.62**	**256.54**	**0.69**	**0.74**	**0.70**	**0.78**
Standard deviation				**127.26**	**126.99**	**144.32**	**130.36**	**123.45**	**0.13**	**0.16**	**0.13**	**0.11**
1500	1	0	0	47.4	39.0	39.5	39.0	39.0	0.82	0.83	0.82	0.82
		0	10	54.0	31.3	32.2	31.3	34.5	0.58	0.60	0.58	0.64
		0	-25	28.1	27.3	27.5	27.3	26.6	0.97	0.98	0.97	0.95
		0	50	28.6	17.5	18.5	17.5	22.0	0.61	0.64	0.61	0.77
		10	0	41.7	36.8	37.2	36.8	36.9	0.88	0.89	0.88	0.89
		100	0	30.5	24.3	24.3	24.3	25.1	0.80	0.80	0.80	0.82
		200	0	22.1	17.6	17.5	17.6	18.5	0.80	0.79	0.80	0.84
		10	10	52.9	29.9	30.6	29.9	33.0	0.56	0.58	0.56	0.62
		100	-25	23.2	19.1	19.1	19.1	18.4	0.82	0.82	0.82	0.79
		200	50	15.4	11.3	11.6	11.3	14.3	0.74	0.76	0.74	0.93
Average				**34.39**	**25.41**	**25.79**	**25.41**	**26.83**	**0.76**	**0.77**	**0.76**	**0.81**
Standard deviation				**13.65**	**9.03**	**9.14**	**9.03**	**8.63**	**0.13**	**0.13**	**0.13**	**0.11**
1500	2	0	0	156.8	129.5	130.9	129.5	129.5	0.83	0.83	0.83	0.83
		0	10	163.0	97.5	100.4	97.5	112.3	0.60	0.62	0.60	0.69
		0	-25	84.0	73.9	74.4	73.9	87.5	0.88	0.89	0.88	1.04
		0	50	65.5	49.1	52.0	49.1	56.9	0.75	0.79	0.75	0.87
		10	0	132.3	121.2	122.5	121.2	122.1	0.92	0.93	0.92	0.92

		100	0	103.3	76.9	77.6	76.9	82.1	0.74	0.75	0.74	0.80
		200	0	76.5	54.7	55.1	54.7	59.8	0.72	0.72	0.72	0.78
		10	10	160.7	92.8	95.4	92.8	107.2	0.58	0.59	0.58	0.67
		100	-25	74.1	53.2	53.5	53.2	60.0	0.72	0.72	0.72	0.81
		200	50	47.4	32.4	33.6	32.4	36.8	0.68	0.71	0.68	0.78
Average				**106.36**	**78.12**	**79.53**	**78.12**	**85.42**	**0.74**	**0.76**	**0.74**	**0.82**
Standard deviation				**43.41**	**31.98**	**32.22**	**31.98**	**31.60**	**0.11**	**0.11**	**0.11**	**0.11**
1500	4	0	0	518.8	408.8	414.9	408.8	408.8	0.79	0.80	0.79	0.79
		0	10	296.6	268.3	270.9	268.3	316.0	0.90	0.91	0.90	1.07
		0	-25	242.7	177.0	178.2	177.0	272.5	0.73	0.73	0.73	1.12
		0	50	140.6	113.0	113.4	113.0	122.6	0.80	0.81	0.80	0.87
		10	0	471.1	374.3	379.5	374.3	384.4	0.79	0.81	0.79	0.82
		100	0	275.7	212.8	214.4	212.8	244.6	0.77	0.78	0.77	0.89
		200	0	184.8	143.8	144.6	143.8	159.5	0.78	0.78	0.78	0.86
		10	10	295.9	253.0	255.3	253.0	299.5	0.86	0.86	0.86	1.01
		100	-25	211.1	126.6	127.1	126.6	183.5	0.60	0.60	0.60	0.87
		200	50	109.8	74.9	75.1	74.9	79.5	0.68	0.68	0.68	0.72
Average				**274.71**	**215.24**	**217.35**	**215.24**	**247.10**	**0.77**	**0.78**	**0.77**	**0.90**
Standard deviation				**132.26**	**111.34**	**113.36**	**111.34**	**109.78**	**0.09**	**0.09**	**0.09**	**0.13**
3000	1	0	0	31.7	26.4	26.5	26.4	26.4	0.83	0.84	0.83	0.83
		0	10	35.4	22.6	22.9	22.6	26.5	0.64	0.65	0.64	0.75
		0	-25	19.6	20.4	20.5	20.4	22.1	1.04	1.05	1.04	1.13
		0	50	20.7	14.4	14.7	14.4	22.0	0.70	0.71	0.70	1.07
		10	0	27.3	25.2	25.3	25.2	25.4	0.92	0.93	0.92	0.93
		100	0	23.3	17.9	17.9	17.9	18.7	0.77	0.77	0.77	0.80
		200	0	18.3	13.6	13.5	13.6	14.1	0.74	0.74	0.74	0.77
		10	10	35.4	21.7	22.0	21.7	25.8	0.61	0.62	0.61	0.73
		100	-25	17.4	14.9	14.9	14.9	15.6	0.86	0.86	0.86	0.90
		200	50	13.6	9.5	9.6	9.5	13.8	0.70	0.70	0.70	1.02
Average				**24.27**	**18.66**	**18.78**	**18.66**	**21.07**	**0.78**	**0.79**	**0.78**	**0.89**

Standard deviation				**7.78**	**5.50**	**5.56**	**5.50**	**5.13**	**0.13**	**0.13**	**0.13**	**0.14**
3000	2	0	0	91.9	86.5	87.0	86.5	86.5	0.94	0.95	0.94	0.94
		0	10	90.1	70.9	71.9	70.9	86.4	0.79	0.80	0.79	0.96
		0	-25	53.1	57.6	57.8	57.6	72.2	1.08	1.09	1.08	1.36
		0	50	47.0	41.3	42.4	41.3	56.2	0.88	0.90	0.88	1.20
		10	0	76.0	82.4	82.8	82.4	83.0	1.08	1.09	1.08	1.09
		100	0	67.2	57.9	57.8	57.9	60.3	0.86	0.86	0.86	0.90
		200	0	54.8	43.5	43.3	43.5	45.1	0.79	0.79	0.79	0.82
		10	10	89.3	68.2	69.0	68.2	83.8	0.76	0.77	0.76	0.94
		100	-25	48.4	43.3	43.3	43.3	50.7	0.90	0.89	0.90	1.05
		200	50	34.8	28.1	28.4	28.1	35.1	0.81	0.82	0.81	1.01
Average				**65.26**	**57.96**	**58.36**	**57.96**	**65.94**	**0.89**	**0.90**	**0.89**	**1.03**
Standard deviation				**20.63**	**19.08**	**19.21**	**19.08**	**18.95**	**0.12**	**0.12**	**0.12**	**0.16**
3000	4	0	0	474.8	247.0	247.0	247.0	247.0	0.52	0.52	0.52	0.52
		0	10	168.4	185.8	185.8	185.8	232.0	1.10	1.10	1.10	1.38
		0	-25	126.1	137.9	137.9	137.9	220.7	1.09	1.09	1.09	1.75
		0	50	92.4	93.4	93.4	93.4	107.6	1.01	1.01	1.01	1.16
		10	0	189.3	231.1	231.1	231.1	240.9	1.22	1.22	1.22	1.27
		100	0	167.3	146.2	146.2	146.2	154.9	0.87	0.87	0.87	0.93
		200	0	133.1	103.8	103.8	103.8	105.9	0.78	0.78	0.78	0.80
		10	10	167.7	176.7	176.7	176.7	216.8	1.05	1.05	1.05	1.29
		100	-25	117.0	99.6	99.6	99.6	148.4	0.85	0.85	0.85	1.27
		200	50	71.4	61.4	61.4	61.4	67.2	0.86	0.86	0.86	0.94
Average				**170.74**	**148.27**	**148.27**	**148.27**	**174.15**	**0.94**	**0.94**	**0.94**	**1.13**
Standard deviation				**113.11**	**61.33**	**61.33**	**61.33**	**65.53**	**0.20**	**0.20**	**0.20**	**0.35**
Average of all 90 results				**129.4**	**98.6**	**101.6**	**99.0**	**110.5**	**0.8**	**0.8**	**0.8**	**0.9**
Standard deviation of all 90 results				**58.52**	**45.89**	**48.38**	**46.27**	**45.53**	**0.13**	**0.13**	**0.13**	**0.14**

Table. A3 Comparison between the results of strength for the beam-column members with $C3$ cross-section (d = 300 mm, b_f = 50 mm, d_1 = 25 mm) obtained from detailed FE models and different design methods.

Length	**Thickness**	**Eccentricity**		**Capacity**					**Ratio of each design method prediction to the detailed FE result**			
L (mm)	**t (mm)**	e_y **(mm)**	e_x **(mm)**	P_{DFE} **(kN)**	P_{DSM} **(kN)**	$P_{DSM,W}$ **(kN)**	$P_{Distortional,W}$ **(kN)**	$P_{Interaction}$ **(kN)**	$\frac{P_{DSM}}{P_{DFE}}$	$\frac{P_{DSM,W}}{P_{DFE}}$	$\frac{P_{Distortional,W}}{P_{DFE}}$	$\frac{P_{Interaction}}{P_{DFE}}$
500	1	0	0	56.0	52.1	52.9	52.1	52.1	0.93	0.94	0.93	0.93
		0	10	60.3	41.1	43.6	41.1	45.3	0.68	0.72	0.68	0.75
		0	-25	39.2	37.6	38.0	37.6	33.7	0.96	0.97	0.96	0.86
		0	50	31.4	22.3	25.5	22.3	25.2	0.71	0.81	0.71	0.80
		10	0	52.8	47.6	48.3	47.6	48.0	0.90	0.92	0.90	0.91
		100	0	30.4	26.8	27.3	26.8	28.9	0.88	0.90	0.88	0.95
		200	0	20.3	18.1	18.4	18.1	19.9	0.89	0.91	0.89	0.98
		10	10	55.8	38.3	40.4	38.3	42.7	0.69	0.73	0.69	0.76
		100	-25	26.9	22.4	22.7	22.4	22.0	0.83	0.84	0.83	0.82
		200	50	18.8	12.4	13.4	12.4	14.2	0.66	0.71	0.66	0.75
Average				**39.17**	**31.87**	**33.05**	**31.87**	**33.21**	**0.81**	**0.85**	**0.81**	**0.85**
Standard deviation				**15.81**	**13.32**	**13.40**	**13.32**	**13.16**	**0.12**	**0.10**	**0.12**	**0.09**
500	2	0	0	199.7	172.8	174.9	172.8	172.8	0.87	0.88	0.87	0.87
		0	10	212.2	128.6	137.7	128.6	136.0	0.61	0.65	0.61	0.64
		0	-25	136.9	90.6	91.9	90.6	110.8	0.66	0.67	0.66	0.81
		0	50	120.4	63.5	74.4	63.5	66.7	0.53	0.62	0.53	0.55
		10	0	191.8	155.4	159.1	155.4	158.4	0.81	0.83	0.81	0.83
		100	0	106.9	81.5	87.6	81.5	89.0	0.76	0.82	0.76	0.83
		200	0	70.7	53.3	58.5	53.3	56.8	0.75	0.83	0.75	0.80
		10	10	197.3	118.7	127.7	118.7	128.1	0.60	0.65	0.60	0.65
		100	-25	97.2	57.1	60.4	57.1	71.3	0.59	0.62	0.59	0.73
		200	50	59.6	34.8	40.3	34.8	37.1	0.58	0.68	0.58	0.62
Average				**139.27**	**95.63**	**101.24**	**95.63**	**102.69**	**0.68**	**0.72**	**0.68**	**0.73**

Standard deviation				**57.08**	**46.38**	**45.96**	**46.38**	**45.60**	**0.11**	**0.10**	**0.11**	**0.11**
500	4	0	0	579.8	502.4	551.1	547.9	502.4	0.87	0.95	0.95	0.87
		0	10	481.7	353.7	377.2	375.7	360.4	0.73	0.78	0.78	0.75
		0	-25	380.8	245.0	256.0	255.3	345.5	0.64	0.67	0.67	0.91
		0	50	249.2	162.0	166.7	166.4	165.7	0.65	0.67	0.67	0.66
		10	0	568.7	444.5	483.5	479.7	456.6	0.78	0.85	0.84	0.80
		100	0	286.3	218.1	229.9	226.2	227.8	0.76	0.80	0.79	0.80
		200	0	183.7	139.3	145.2	142.5	143.9	0.76	0.79	0.78	0.78
		10	10	475.3	324.0	344.3	342.3	335.6	0.68	0.72	0.72	0.71
		100	-25	293.7	149.8	155.2	153.6	190.8	0.51	0.53	0.52	0.65
		200	50	150.1	88.0	90.3	89.3	91.6	0.59	0.60	0.59	0.61
Average				**364.94**	**262.66**	**279.95**	**277.89**	**282.03**	**0.70**	**0.74**	**0.73**	**0.75**
Standard deviation				**155.42**	**138.85**	**154.23**	**153.58**	**138.34**	**0.10**	**0.12**	**0.12**	**0.10**
1500	1	0	0	54.9	46.6	46.0	46.6	46.6	0.85	0.84	0.85	0.85
		0	10	49.5	37.6	38.7	37.6	43.0	0.76	0.78	0.76	0.87
		0	-25	35.8	34.6	34.3	34.6	33.4	0.97	0.96	0.97	0.93
		0	50	25.2	21.2	23.8	21.2	25.2	0.84	0.94	0.84	1.00
		10	0	47.6	42.9	42.5	42.9	44.0	0.90	0.89	0.90	0.92
		100	0	26.9	25.3	25.2	25.3	28.6	0.94	0.94	0.94	1.06
		200	0	17.1	17.4	17.4	17.4	19.9	1.02	1.02	1.02	1.16
		10	10	45.5	35.2	36.2	35.2	40.8	0.77	0.80	0.77	0.90
		100	-25	25.2	21.3	21.2	21.3	21.9	0.85	0.84	0.85	0.87
		200	50	13.7	12.0	12.8	12.0	15.2	0.88	0.94	0.88	1.11
Average				**34.13**	**29.40**	**29.81**	**29.40**	**31.86**	**0.88**	**0.89**	**0.88**	**0.97**
Standard deviation				**14.54**	**11.56**	**11.24**	**11.56**	**11.28**	**0.08**	**0.08**	**0.08**	**0.11**
1500	2	0	0	189.8	153.6	151.6	153.6	153.6	0.81	0.80	0.81	0.81
		0	10	185.8	117.6	120.8	117.6	136.0	0.63	0.65	0.63	0.73
		0	-25	116.9	85.0	84.2	85.0	109.7	0.73	0.72	0.73	0.94
		0	50	81.7	60.7	66.6	60.7	66.7	0.74	0.82	0.74	0.82
		10	0	172.7	139.7	138.8	139.7	144.9	0.81	0.80	0.81	0.84

		100	0	104.0	77.0	78.7	77.0	89.0	0.74	0.76	0.74	0.86
		200	0	67.3	51.4	53.1	51.4	56.8	0.76	0.79	0.76	0.84
		10	10	179.8	109.3	112.5	109.3	128.1	0.61	0.63	0.61	0.71
		100	-25	89.8	54.8	55.6	54.8	70.9	0.61	0.62	0.61	0.79
		200	50	51.5	34.0	36.7	34.0	37.1	0.66	0.71	0.66	0.72
Average				**123.94**	**88.30**	**89.86**	**88.30**	**99.28**	**0.71**	**0.73**	**0.71**	**0.81**
Standard deviation				**53.25**	**40.18**	**39.06**	**40.18**	**40.77**	**0.08**	**0.08**	**0.08**	**0.07**
1500	4	0	0	568.0	483.3	476.1	483.3	483.3	0.85	0.84	0.85	0.85
		0	10	399.5	344.1	340.5	344.1	360.4	0.86	0.85	0.86	0.90
		0	-25	320.7	240.3	238.5	240.3	342.3	0.75	0.74	0.75	1.07
		0	50	200.2	159.9	159.1	159.9	165.7	0.80	0.79	0.80	0.83
		10	0	513.1	429.4	424.8	429.4	450.7	0.84	0.83	0.84	0.88
		100	0	264.6	214.4	215.7	214.4	227.8	0.81	0.82	0.81	0.86
		200	0	171.2	137.7	139.5	137.7	143.9	0.80	0.81	0.80	0.84
		10	10	395.8	315.9	313.4	315.9	335.6	0.80	0.79	0.80	0.85
		100	-25	255.2	148.0	148.6	148.0	189.5	0.58	0.58	0.58	0.74
		200	50	120.5	87.4	88.1	87.4	91.5	0.73	0.73	0.73	0.76
Average				**320.88**	**256.05**	**254.43**	**256.05**	**279.07**	**0.78**	**0.78**	**0.78**	**0.86**
Standard deviation				**146.96**	**132.65**	**129.93**	**132.65**	**134.14**	**0.08**	**0.08**	**0.08**	**0.09**
3000	1	0	0	45.4	31.8	31.3	31.8	31.8	0.70	0.69	0.70	0.70
		0	10	45.7	27.3	27.6	27.3	32.1	0.60	0.60	0.60	0.70
		0	-25	28.6	25.7	25.4	25.7	30.4	0.90	0.89	0.90	1.06
		0	50	22.7	17.5	18.6	17.5	25.2	0.77	0.82	0.77	1.11
		10	0	38.9	30.0	29.6	30.0	31.6	0.77	0.76	0.77	0.81
		100	0	20.3	19.8	19.7	19.8	24.2	0.98	0.97	0.98	1.19
		200	0	11.4	14.4	14.4	14.4	17.4	1.27	1.26	1.27	1.53
		10	10	44.2	26.0	26.2	26.0	31.4	0.59	0.59	0.59	0.71
		100	-25	21.8	17.3	17.2	17.3	20.2	0.79	0.79	0.79	0.92
		200	50	12.4	10.5	11.0	10.5	13.4	0.85	0.89	0.85	1.08
Average				**29.13**	**22.04**	**22.09**	**22.04**	**25.76**	**0.82**	**0.83**	**0.82**	**0.98**

Standard deviation				**13.46**	**7.10**	**6.86**	**7.10**	**6.83**	**0.20**	**0.20**	**0.20**	**0.27**
3000	2	0	0	185.5	104.1	102.5	104.1	104.1	0.56	0.55	0.56	0.56
		0	10	132.8	86.2	86.1	86.2	103.6	0.65	0.65	0.65	0.78
		0	-25	85.0	67.3	66.5	67.3	101.1	0.79	0.78	0.79	1.19
		0	50	65.6	51.1	52.5	51.1	66.7	0.78	0.80	0.78	1.02
		10	0	126.8	97.5	96.5	97.5	103.3	0.77	0.76	0.77	0.81
		100	0	94.2	62.2	62.9	62.2	77.7	0.66	0.67	0.66	0.82
		200	0	65.5	44.3	45.3	44.3	55.4	0.68	0.69	0.68	0.85
		10	10	134.1	81.6	81.8	81.6	101.1	0.61	0.61	0.61	0.75
		100	-25	71.6	46.9	47.2	46.9	65.3	0.65	0.66	0.65	0.91
		200	50	40.0	30.7	31.9	30.7	37.1	0.77	0.80	0.77	0.93
Average				**100.11**	**67.18**	**67.31**	**67.18**	**81.53**	**0.69**	**0.70**	**0.69**	**0.86**
Standard deviation				**43.85**	**24.48**	**23.66**	**24.48**	**24.47**	**0.08**	**0.09**	**0.08**	**0.17**
3000	4	0	0	527.1	288.6	288.6	288.6	288.6	0.55	0.55	0.55	0.55
		0	10	263.3	229.3	229.3	229.3	250.3	0.87	0.87	0.87	0.95
		0	-25	223.2	180.0	180.0	180.0	313.1	0.81	0.81	0.81	1.40
		0	50	148.1	125.8	125.8	125.8	140.4	0.85	0.85	0.85	0.95
		10	0	355.6	267.6	267.6	267.6	283.1	0.75	0.75	0.75	0.80
		100	0	237.3	161.6	161.6	161.6	183.3	0.68	0.68	0.68	0.77
		200	0	148.1	112.2	112.2	112.2	121.7	0.76	0.76	0.76	0.82
		10	10	263.4	215.8	215.8	215.8	239.0	0.82	0.82	0.82	0.91
		100	-25	184.5	120.8	120.8	120.8	167.7	0.65	0.65	0.65	0.91
		200	50	94.8	74.6	74.6	74.6	81.3	0.79	0.79	0.79	0.86
Average				**244.53**	**177.61**	**177.61**	**177.61**	**206.85**	**0.75**	**0.75**	**0.75**	**0.89**
Standard deviation				**123.84**	**71.20**	**71.20**	**71.20**	**79.05**	**0.10**	**0.10**	**0.10**	**0.21**
Average of all 90 results				**155.12**	**114.53**	**117.26**	**116.22**	**126.92**	**0.76**	**0.78**	**0.76**	**0.86**
Standard deviation of all 90 results				**69.36**	**53.97**	**55.06**	**55.61**	**54.85**	**0.11**	**0.10**	**0.11**	**0.13**